Master thesis

Spot Weldability of TRIP Steel with High Carbon, High Aluminium Content

Jung, Geunsu (鄭根洙)

Computational Metallurgy

Graduate Institute of Ferrous Technology

Pohang University of Science and Technology

2011

고 탄소, 알루미늄 합금 TRIP강의 점용접성 평가

Spot Weldability of TRIP Steel with High Carbon, High Aluminium Content

Spot Weldability of TRIP Steel with High Carbon, High Aluminium Content

By

Jung, Geunsu
Computational Metallurgy
Graduate Institute of Ferrous Technology
Pohang University of Science and Technology

A thesis submitted to the faculty of Pohang University of Science and Technology in partial fulfillments of the requirements for the degree of Master of Science in the Graduate Institute of Ferrous Technology (Computational Metallurgy)
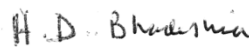
Pohang, Korea
December 19th, 2011

Approved by

Prof. Suh, Dong-Woo

Dongwoo Suh

Major Advisor

Prof. Bhadeshia, H.K.D.H.

H.D. Bhadeshia

Co-Advisor

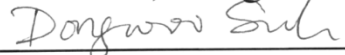# Spot Weldability of TRIP Steel with High Carbon, High Aluminium Content

Jung, Geunsu

This dissertation is submitted for the degree of Master of Science at the Graduate Institute of Ferrous Technology of Pohang University of Science and Technology. The research reported herein was approved by the committee of Thesis Appraisal.

December 19th, 2011

Thesis Review Committee
Chairman: Prof. Suh, Dong-Woo
(Signature) _Dongwoo Suh_
Member: Prof. Lee, Jong-bong
(Signature) _____
Member: Prof. B. C. De Cooman
(Signature) _Bruno D. Cooman_

Abstract

Recent trends towards the integration of strong steels into the automotive industry have accentuated demands on their resistance spot weldability, a technique most widely used for bonding during automotive assembly. However, strong steels are inherently rich in alloying elements. TRIP steels are not exceptions because they require certain level of carbon content and cementite inhibitors such as silicon to maintain austenite stability. The resulting high hardenability makes it difficult to avoid the formation of brittle martensite in the heat affected zone of resistance spot welds.

  Recent research on TRIP-assisted steel alloy with relatively high carbon and aluminium concentration showed a possible way forward. In this so called δ-TRIP steel, δ-ferrite is stabilized by aluminium and persists in the microstructure at all temperatures after solidification. Soft δ-ferrite can be retained in the martensite that forms. Since it is assumed that avoiding fully martensitic weld nugget may be helpful for better weldability and weld toughness, this idea is promising. Previous research done by Yi et al. reports that δ-ferrite retained after welding process is indeed good for better spot weldabilty, but it is not clear whether the properties achieved are adequate.

Expanding on this notion, the effectiveness of δ-ferrite in terms of spot weldability has been qualitatively investigated in this work with alloys newly designed for the purpose. The thesis can be divided into two parts, pre-weld studies and an understanding of the weld. The initial part deals with the optimization of heat treatment conditions itself to acquire the best possible mechanical properties for the alloys. Specimens were tensile tested and analyzed using optical and electron microscopes. The weld study covers microstructure, joint property evaluations and fracture surface analysis. Relations between weld microstructure and fracture mechanisms have been obtained. To further enhance spot weldability, additional heating processes after spot welding with different conditions were applied to assess whether the tempering of martensite in the weld nuggets is advantageous. The procedure was expected to soften the weld nugget and result in better weld integrity.

Nomenclature

AHSS	Advanced high strength steel
HSS	High strength steel
TRIP	Transformation induced plasticity
IF steel	Interstitial free steel
Ac1	Temperature of austenite formation on heating
Ac3	Temperature at which transformation of ferrite into austenite is completed on heating
RSW	Resistance spot welding
TS	Tensile strength
UTS	Ultimate tensile strength
YS	Yield strength
MPa	Mega pascal, the unit for tensile strength
TSS	Tensile shear strength
CTS	Cross tensile sterngth
kVA	Kilo volt-ampere
WS_{min}	Minimum weld nugget size
AC	Alternating current
DC	Direct current

Table of contents

List of Figures

List of Tables

x

1 Introduction

1.1 TRIP steels and δ-TRIP steel

Competition between materials and environmental legislation are driving the big trend for lighter automobile. The exploitation of stronger steel is therefore a common practice in industry. Among many kinds of high-strength steels, TRIP steel stands out because of its excellent formability and strength-ductility ratio [1].

In TRIP steel, some austenite, usually stable only at high temperatures, is retained to the ambient temperature but transforms into hard martensite during straining, which delays the onset of necking, resulting in greater uniform elongation [2]. Therefore, retained austenite is important in determining the mechanical properties of TRIP steel.

Conventional low-alloyed TRIP assisted steels has 0.15 C, 1.2-1.5 Mn and 1.0-1.5 Si wt% in composition [3]. The addition of at least 0.3-0.8 wt% Si addition is common as a cementite inhibitor [2, 3]. However, silicon has been reported to reduce surface quality by forming Si oxide phases [4].

In order to retain enough austenite for good mechanical properties and at the same time improve surface quality, many alloy designs have been made where silicon were replaced by aluminium with the function of inhibiting cementite formation [3]. Recently, a new type of TRIP steel with significant aluminium

content has been suggested and developed whose mechanical properties were outstanding with ultimate tensile strength of more than 1 GPa and uniform elongation in excess of 23% [5, 6]. This so called δ-TRIP steel characterizes itself by having δ-ferrite which is stable at all temperatures in the solid state. This kind of TRIP steel has been investigated by authors [5-10] and is described in detail in the next chapter.

1.2 Resistnace spot welding

This is a simple and quick metal-bonding method in use by industry [11]. In automotive assembly, more than 3,000 spots are typically made for the structure of a single vehicle [9, 12]. The conventional process starts with clamping the metal sheets in between electrodes as in Fig. 1.1. When the electrical current coming from one electrode travels through the sheets, heat is created at the interface between electrodes and sheets where the electrical resistance is large. With this localized heat due to contact, metal starts to melt, and the weld nugget is created under high pressures pushing two sheets together. After certain holding time, metal sheets are released bound and the whole process ends. Usually the entire sequence takes less than 1 s, so spot welding is a rapid and productive welding method. Depending on the thickness and type of the metal, welding conditions such as weld current, weld time, electrode type and electrode force should be adjusted.
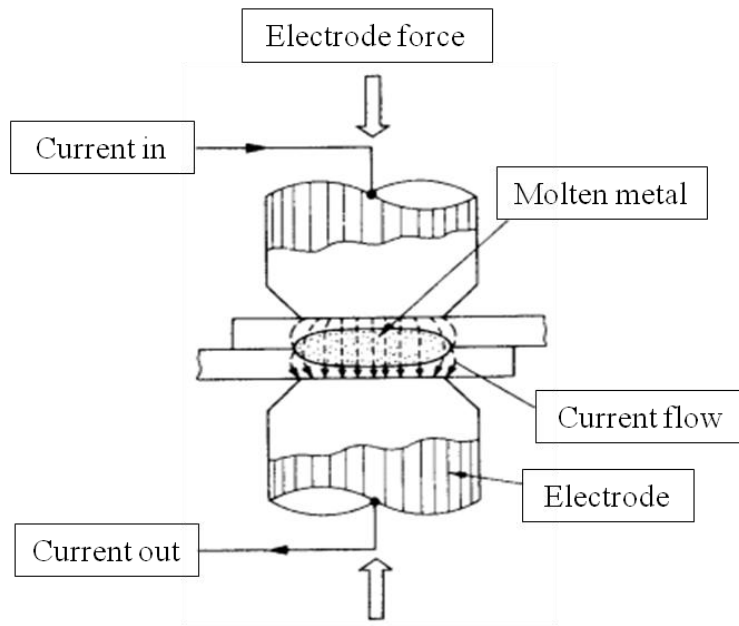
Fig. 1.1 schematic of spot welding process

1.3 Objectives

Since steel sheets that are made for the use in the automotive industry are eventually spot-welded in the production process, weldability of the steel must be assessed before application. In most cases, higher strength in strong steels comes from enhanced alloying element concentrations. This may bring about a reduction in weldability because of an increased carbon equivalent [13]. It becomes clear that when conducting an alloy design, not only mechanical properties of the steel but also its spot weldability should be taken into account [13, 14]. Although δ-TRIP has a high carbon equivalent, retained δ-ferrite in the weld zone and heat affected zone due to its high aluminium concentration helps

improve weld toughness.

Alloys that are investigated in this work had been modelled based on this idea of utilizing δ-ferrite for better weld performance of the steel. Thus, the objectives of this thesis can be stated as below.

1) Optimization of heat treatment parameters for the alloys for the best mechanical properties before actual welding

2) Investigation on the influence of δ-ferrite on spot weldabiilty in the newly proposed TRIP-assisted steels

3) Analysis of weld microstructures and qualitative study of δ-ferrite formation in the fusion zone

4) Study of weld fracture surfaces and fracture mechanisms

2 Literature review

2.1 TRIP steel

The need for strong steels for the automotive industry has exerted for many decades [3, 15], in order to achieve weight reduction, to enhance safety and to avoid any threat from alternative materials such as aluminium.

Alloys with tensile strength in excess of 600 MPa and elongation of around 30% (Fig. 2.1), are ideal for meeting these needs. TRIP-assisted steels are excellent in this context, having a balance of strength and ductility which permits complex shaping operations during the manufacture of components.

IF: Interstitial free steel
BH: Bake hardenable steel
CMn: Plane C-Mn steel
HSLA: High strength low alloyed steel
DP: Dual phase steel
CP: Complex phase steel
TRIP: Transformation induced plasticity steel
MS: Martensitic grade of steel
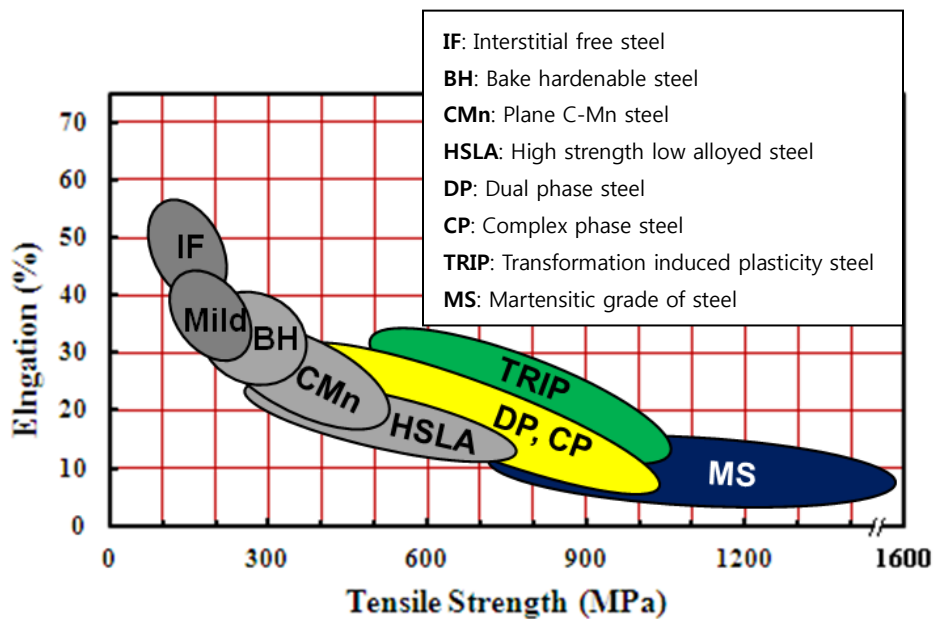
Fig. 2.1 mechanical properties of automotive steel [16]

Fig. 2.2 illustrates the TRIP phenomenon wherein retained austenite transforms into martensite under loading, thus suppressing plastic instability and extending the range of uniform elongation [17, 18]. Fully austenitic TRIP steels do exist but require large quantities of austenite stabilizing solutes and hence are not affordable. However, as can be seen in Fig. 2.3, conventional low-alloy TRIP-assisted steel has austenite only as a minor phase dispersed in a rather soft ferrite matrix [19].
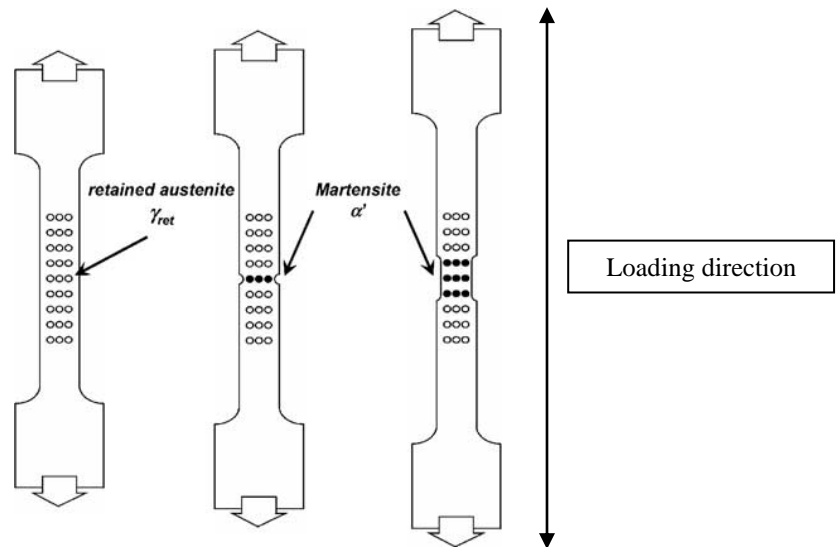
Fig. 2.2 an illustration of TRIP phenomena [18]
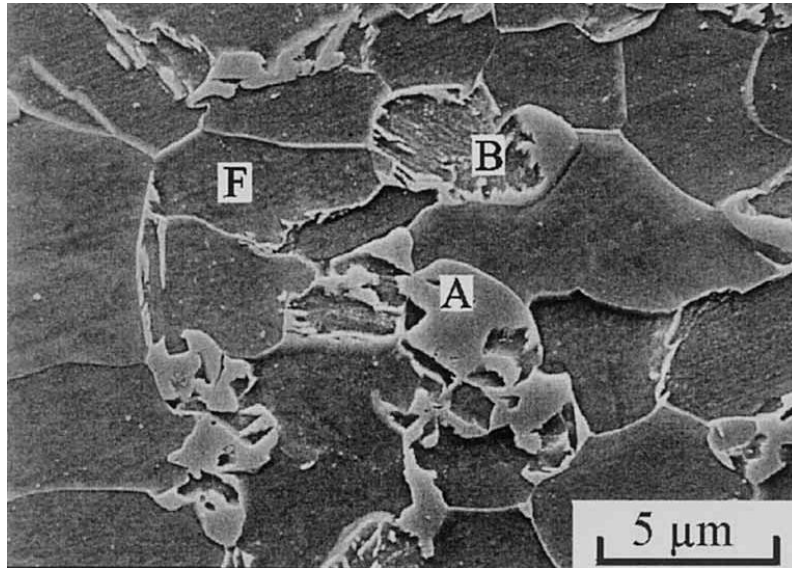
Fig. 2.3 an example of the multiple phase microstructure of conventional TRIP-assisted steel with a composition of 0.11 C, 0.15 Mn, 0.15 Si, 0.04 Al wt% (F: ferrite A: austenite B: bainite) [20]

As shown in Fig. 2.4, a heating process for TRIP steels generally consists of 3 stages; intercritical annealing, isothermal transformation and the final cooling. The intercritical annealing is usually done in between the Ac1 and Ac3 temperatures where two phases, ferrite and austenite, are thermodynamically stable. After, the steel is rapidly cooled to the temperature range where bainitic transformation proceeds and as a result carbon partitions into the residual austenite [20]. The carbon-enrichment of the austenite is preserved by adding cementite retarders such as silicon, which deter the precipitation of cementite from austenite [21]. Consequently, the enriched austenite becomes stable and can

survive martensite transformation to room temperature [3, 22].
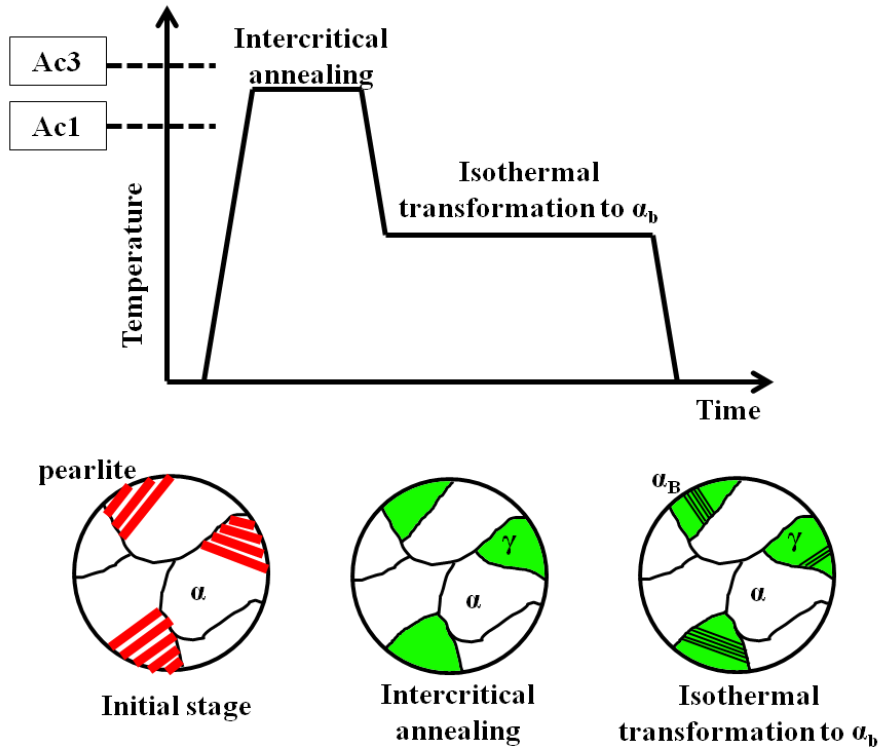
Fig. 2.4 typical heat treatment cycle for modern TRIP steel and schematics of expected microstructure at each stage (α: ferrite γ: austenite α_B: bainite)

Although the addition of silicon is necessary to saturate austenite with carbon by preventing carbide nucleation in conventional TRIP steels, the oxide of silicon, SiO_2, on steel surface can cause some problems. For the prevention of corrosion, Zn coating is usually applied to automotive steel sheets, but silicon selectively oxidizes and forms SiO_2 on steel surfaces, deteriorating molten zinc wettability

[4, 23, 24]. Moreover, the silicon oxide is known to anchor iron oxide which in turn forms red-scale on steel surface, making it difficult to remove oxide layers by acid pickling after hot-rolling process [25, 26].

Recently, deviating from the conventional CMnSi TRIP steels in composition, new variations of TRIP steels with silicon largely substituted by aluminium have been actively investigated, partly to cope with the problems of galvanizability [20, 27-31].

Although the effect of aluminium in terms of the retardation of cementite formation is similar to that of silicon, solid solution strengthening by aluminium is found to be not as great as by silicon [20, 29, 32, 33]. Suh et al., reported that partial substitution of silicon by aluminium alters the free energy relations of ferrite and austenite transformation and, thus, encourages ferrite formation from austenite after intercritical annealing [30].

2.2 δ-TRIP steel

Lately, by means of a neural network method, an attempt has been made to develop TRIP steels with the aim of keeping silicon to a minimum, while optimizing austenite stability with a higher than usual carbon concentration [5, 6]. This work led to a variety of "δ-TRIP" steel. The neural network method is a nonlinear regression method and details are described elsewhere [34, 35]. An initial net of input variables for the neural network consisted of a base steel composition of 0.2 C, 15.5 Mn, 1.0 Si, 0.5 Al, 0.02 P wt%, intercritical annealing

parameters of 780℃ for 300 s and isothermal holding parameters of 400℃ for 500 s [6]. Fig. 2.5 illustrates several examples of the trends predicted by calculation. It was predicted that carbon and manganese help retain more austenite. Silicon and aluminium also increase the fraction of residual austenite because they suppress cementite formation during isothermal holding process [2, 3, 21]. Based on such predictions, an ideal TRIP steel in which enough residual austenite is obtained and the amount of solute silicon is kept minimum was estimated with the neural network method along with a commercially available genetic algorithm [36]. The composition of which is 0.4 C, 2.0 Mn, 0.5 Si, 2.0 Al, 0.5 Cu, 0.02 P wt%. The steel is expected to have 41±20 vol% of retained austenite fraction after the intercritical annealing at 840℃ for 60 s followed by isothermal holding at 300℃ for 900 s [6].

As it can be expected from the steel's calculated phase diagram, δ-ferrite does not completely disappear on solidification, persisting to a minimum 20 vol% at ambient temperature. Fig 2.7 shows the dendritic δ-ferrite in the microstructure of δ-TRIP steel, and this is a unique feature of the steel.

This new δ-TRIP steel has been reported to have an ultimate tensile strength of 1 GPa and total elongation of more than 20% if properly heat treated [6], and from Fig 2.8, it is clear that its mechanical properties are comparable with conventional TRIP steels.
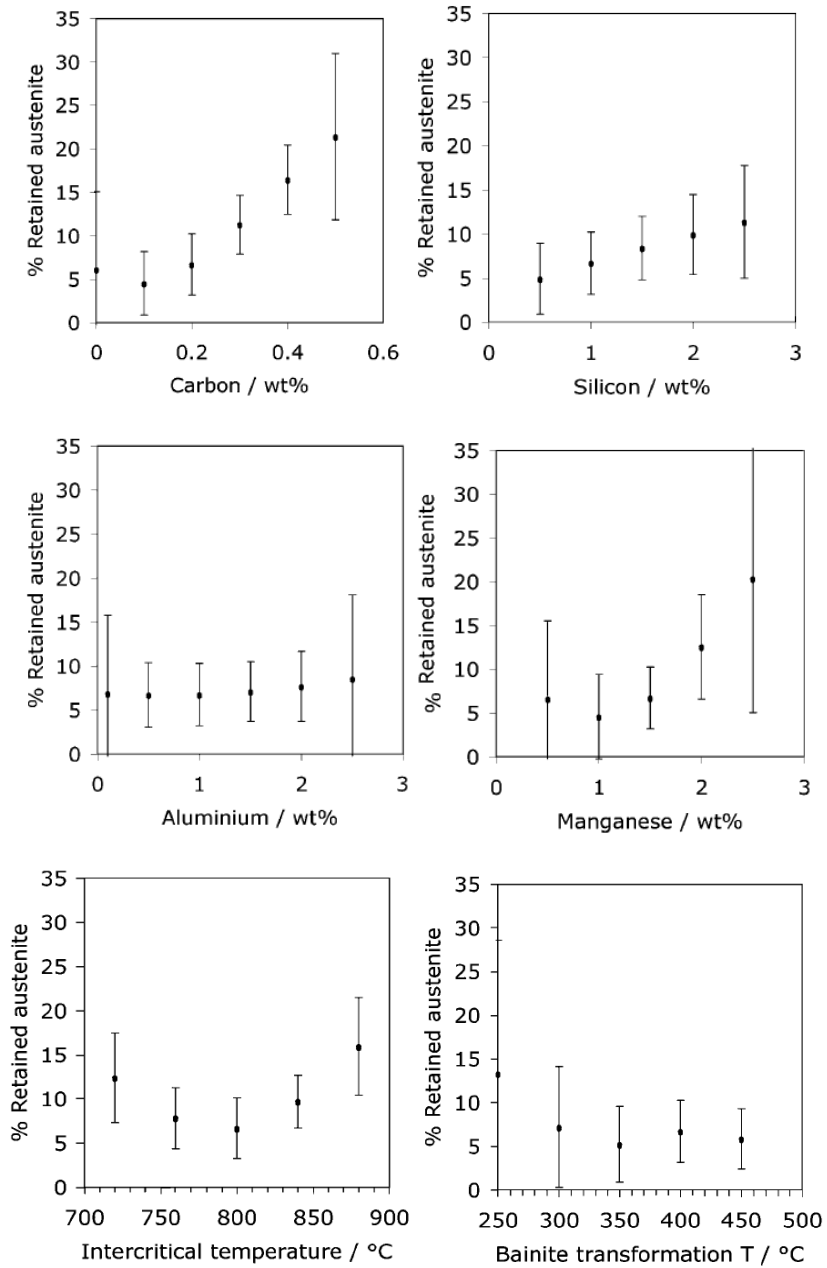
Fig. 2.5 trends of the effect of alloying elements on the amount of retained austenite % [6]
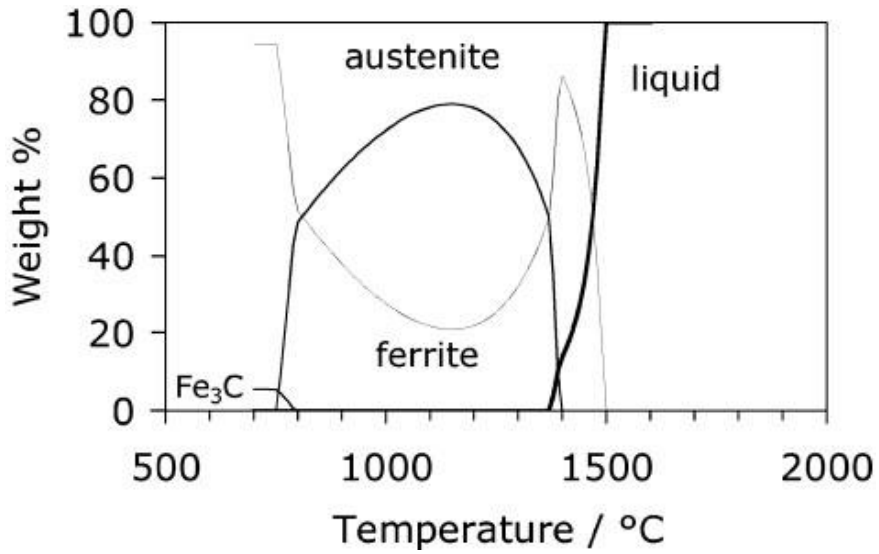
Fig. 2.6 predicted quantities of each phase as a function of temperature for the optimized alloy [6]
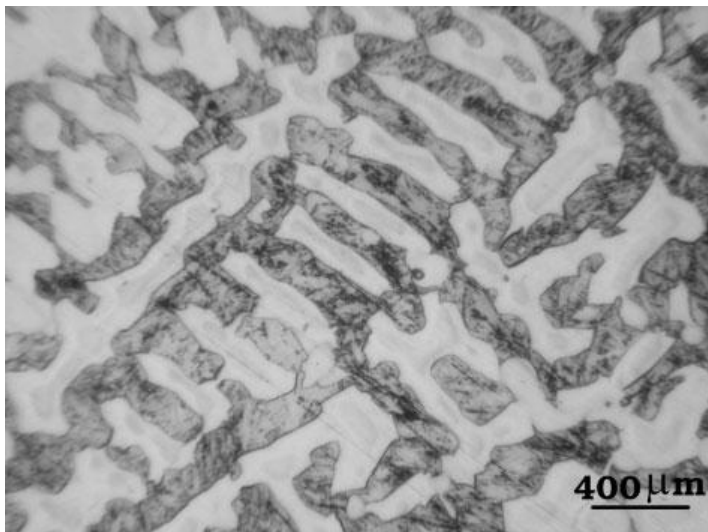
Fig. 2.7 δ-ferrite dendrite in microstructure of δ-TRIP steel [6]
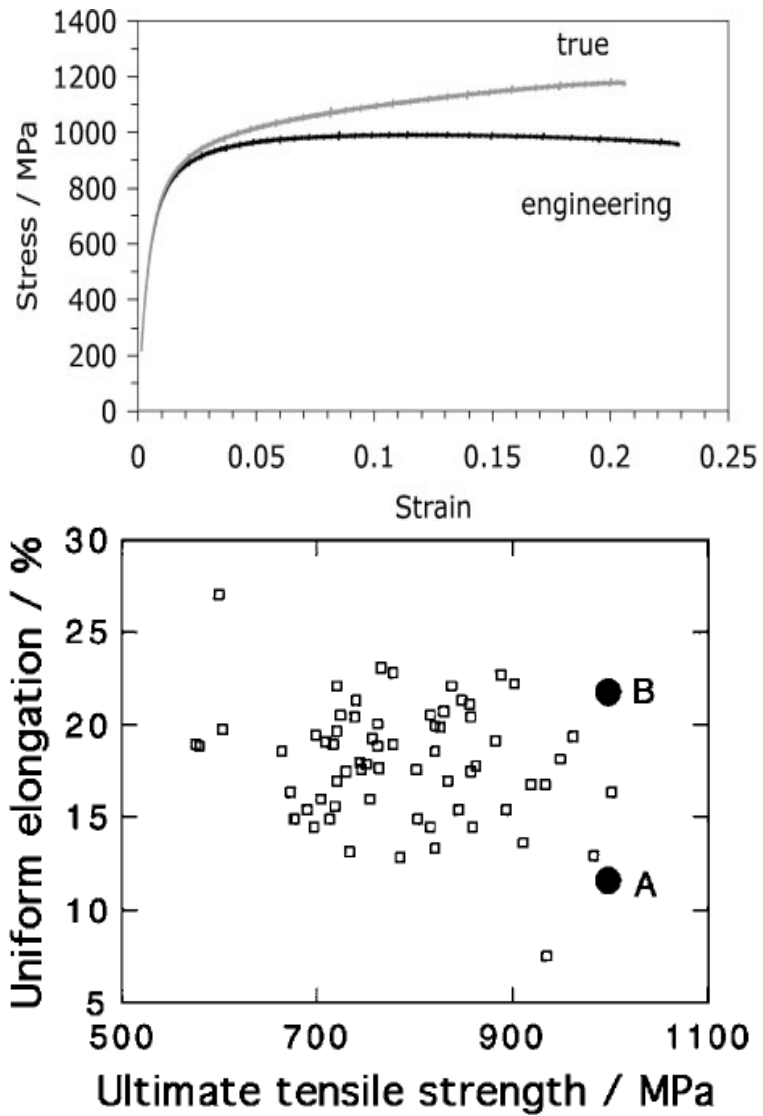
Fig. 2.8 a stress-strain curve of new δ-TRIP steel (heated at 940℃ for 12 h and isothermally heat treated at 300℃ for 3 h) above, the comparison of properties against other TRIP steels from literature below, black dots from new δ-TRIP steel, 'A' represents uniform elongation and 'B' total elongation [6]

By means of neural network modeling process with genetic algorithm, δ-TRIP steel had been developed, and further work has been reported with respect to its retention [7-10]. A distinguishing aspect of this novel steel is the retention of δ-ferrite following solidification process, which may possibly improve weldability of the steel by preventing fully martensitic weld zones. The directly welded part of the steel melts and solidifies again, which in most cases for AHSS, ends of a highly brittle martensitic weld nugget. However, if the δ-ferrite survives in the nugget zone, then it well reduces the weld hardness and hence embrittlement. This has partly been investigated by Yi et al. [9], although detailed relationships between δ-ferrite, weld fracture mechanism and weldabilty remains unclear.

2.3 Resistance Spot Welding

2.3.1 Introduction of resistance spot weld

Resistance spot welding, RSW in short, is simple, easy to automate and fit for mass production, and for these reasons it is one of most widely used joining methods in the automotive industry. RSW is an autogenous welding process, meaning that unlike other methods, it does not require filler metals. RSW harnesses the metal's natural electrical resistance to generate heating. The procedure begins with electrodes which clamp two metal sheets (Fig. 2.9). The current flows through the sheets from one electrode to the other, and resistance to this flowing current generates heat. A temperature is reached where the metal sheets fuse at the faying surfaces and a molten region is generated in between

two sheets. As the current shuts off, the melt rapidly solidifies due to cooling water, forming a solid nugget. Ever since the original invention by Professor Elihu Thomson in 1877, the process has been applied actively for the assembly of metal sheets in the automobile and aircraft industries [37].
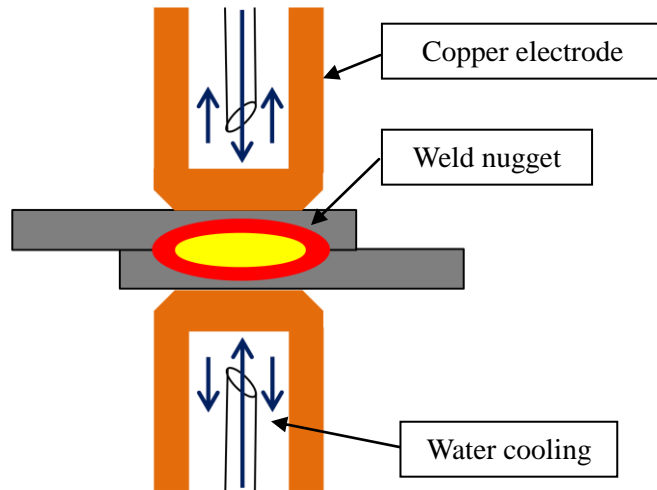
Fig 2.9 a schematic of RSW process

The heat generated by resistance is expressed as below [13].

$$Q \propto (R_1 + R_2) \cdot I^2 \cdot s \cdot r^{-4} \qquad (2.3.1)$$

Here R_1 is the contact resistance of two metal sheets, R_2 the metal's electrical resistance, I the weld current, s the weld time and r the contact diameter of two sheets. R_1 and R_2 are approximately constant, so the current, weld time and contact diameter determined by the electrical force are known to be important in determining the welding condition [13]. Thus, manipulation of such welding

parameters for each material is the key for controlling weld quality.

2.3.2 Weld parameters

During welding, molten zone at the faying sheet surface becomes the weld nugget, so if more heat can be generated, a larger volume of metal can be melted, resulting in a bigger nugget. Larger weld nuggets are generally good for weld performance [38-40]. The weld nugget size should be large enough for better impact property as well as preferable weld failure mode [38, 40].

Current

In RSW, the generated heat is proportional directly to the weld current. Two types of current wave forms are available for conventional RSW processes; they are AC (alternating current) and DC (direct current) wave forms. In the automotive industry, the spot welding process with single-phase AC has been predominant [41]. DC systems can be used by rectification of single-phase or multi-phase AC into DC. Inverter equipped spot welders can provide very high frequency (2000 Hz) DC, which is effective in terms of energy use [41]. Also, DC system-based spot welding usually requires more equipment, thus bringing reliability problems, and is more costly [42], but it minimizes the heat loss and provides uniform heat flow. Fig. 2.10 compares each current wave form, and in a single-phase AC there is an inevitable energy loss because of a series of current zero points, while DC systems provide reliable uniform heat flow. Many

investigations on the differences that may come from different power systems, AC or DC, have been conducted by many authors [41, 43].
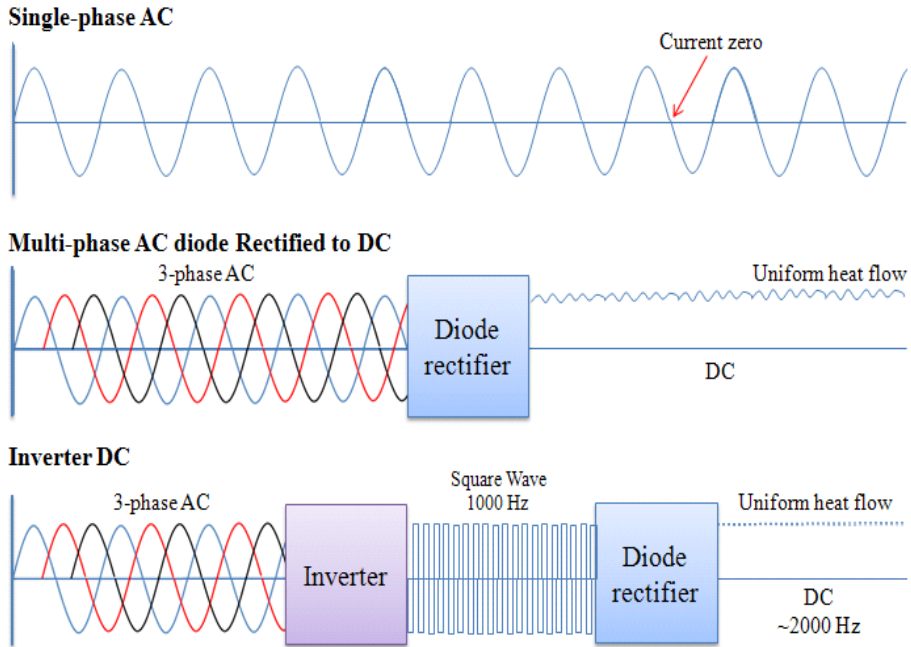
Fig. 2.10 comparison of different welding current wave forms

Resistance

Although practically uncontrollable, it is important to understand the effect of resistance on weldability in RSW. Fig. 2.11 illustrates regions where electrical resistivity exists in RSW, and it can be observed that there are two major types, bulk and contact resistance. The total is then the sum of all the resistance values which are in series. Bulk resistance largely is the characteristic of the sheet material that is spot welded. For most metals, it increases with temperature, and a

stiff peak is observed for aluminium at 925 K, the melting point of the metal (Fig. 2.12).
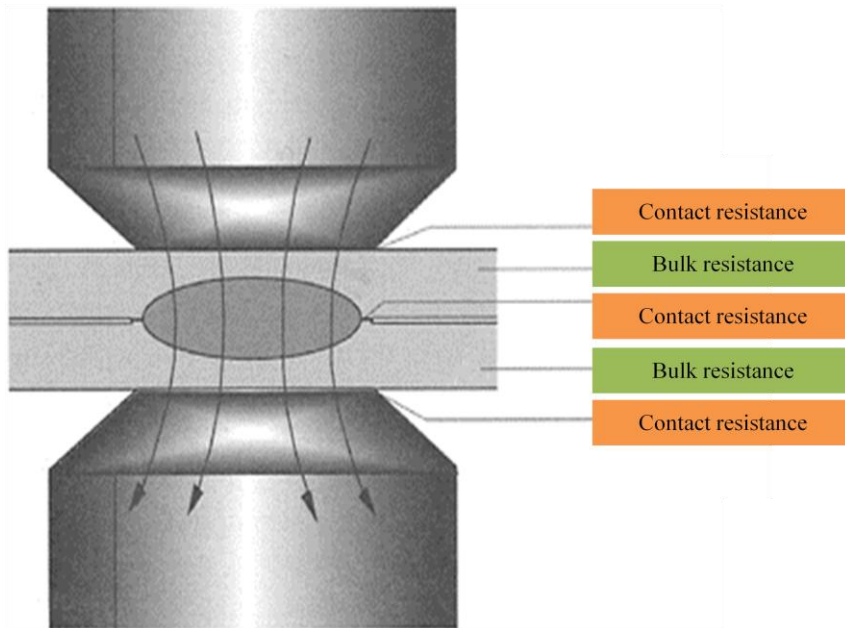
Fig. 2.11 resistance in general spot welding process [44]
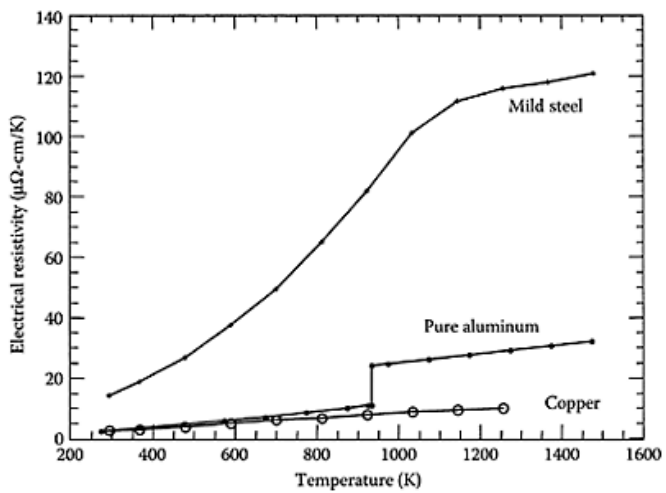
Fig. 2.12 change in resistivity with temperature for different metals [44]

Contact resistance is significantly affected by pressure and surface condition. Brown measured resistance change during spot welding (Fig. 2.13). In the case of AC welding, resistance drops rapidly at the initial stage because of the decreased contact resistance from the high current peak that is absent in DC. Highly concentrated current generates great heat and brakes down the contact surface, destroying possible oxide phases on surface that can act as insulators [41]. As a result, heating efficiency in spot weld process can be compromised for AC welding. Later, because of the fact that bulk resistance increase in proportion to temperature, the overall resistance of AC eventually approaches to that of DC. Fig. 2.14 is the comparison of contact resistance profiles of AC and DC welding suggested by Li et al., and it shows a rapid drop of contact resistance in the case of AC welding [42].
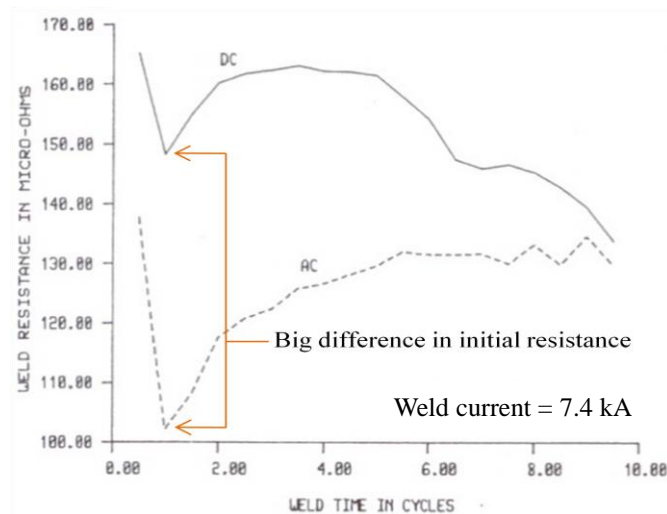
Fig. 2. 13 dynamic resistance curves for 10-cycle AC and DC welds on 0.037-in. uncoated steel [41]
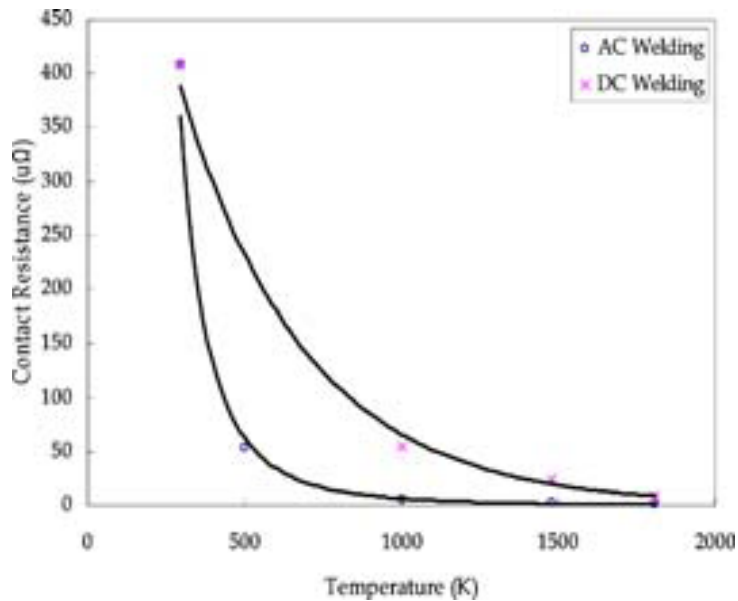
Fig. 2.14 contact resistance comparison of AC and DC welding [42]

Weld time

Spot welding process generally consists of 4 steps, which are squeezing, welding, holding and final releasing [11]. In AC systems, the weld time is expressed in cycles (one cycle is 1/60 of a second in a 60 Hz power system), while millisecond is used for DC systems. During squeeze time, metal sheets are placed in position and clamped by electrodes. When the electrode force has reached the desired level, welding proceeds by the application of current. During this time, melting and joining occurs. Weld time should be determined according to material type, weld quality as well as productivity. The current is shut off during the hold time, so the nugget is allowed to cool. Finally the metal is released, and the next welding sequence begins. The time for each step should be

20

set according to the material, thickness and the coating conditions [45].

Electrode force

Electrode force is applied on electrodes to press and secure metal sheets in position. Electrode force P is expressed as below, where t is the metal thickness in mm, TS tensile strength of the steel sheets in MPa [13].

$$P = 2.45 \cdot t \cdot \left(\frac{TS}{300}\right)^{0.5} \qquad (2.3.2)$$

According to the above equation, stronger steels will require greater electrode force. If the force is insufficient to push the two metal sheets tight, a small contact diameter results, which alters the amount of heat that is generated, according to equation 2.3.1.

Weld lobe curve

Fig. 2.15 demonstrates the general type of weld-lobe curve diagram. This diagram simply shows the window of operation within which weld quality can be guaranteed. Although many variations of the lobe diagram can exist, the electrode force is customarily set constant, and the diagram is drawn on the basis of current versus time.

The lower boundary in the graph is determined at the condition in which the weld current is not high enough, so weld nugget size would not grow as big as minimum weld nugget size, which is $4t^{0.5}$ (t=metal sheet thickness). Criteria for

the minimum nugget size may vary depending on the standards and applications for example $5t^{0.5}$ for more severe condition. Sun explained that the conventionally suggested minimum weld nugget size $4t^{0.5}$ is insufficient to guarantee spot weldability for 800 grade high steels [38]. Marya came up with a new and stricter criterion for determining minimum weld size, and it is expressed as [40],

$$\varphi(\text{mm}) \geq 2.7d(\text{mm}) + 1.6 \qquad (2.3.3)$$

where φ is a weld nugget diameter, and d is the sheet thickness.

The upper boundary is drawn from the points over which expulsion occurs. Expulsion is one kind of a weld defect and leads to the loss of metal, so it is detrimental to weld quality [44]. Different materials have different weld conditions, so different lobe curves. For weld quality, welding should be done within the range of two boundaries.
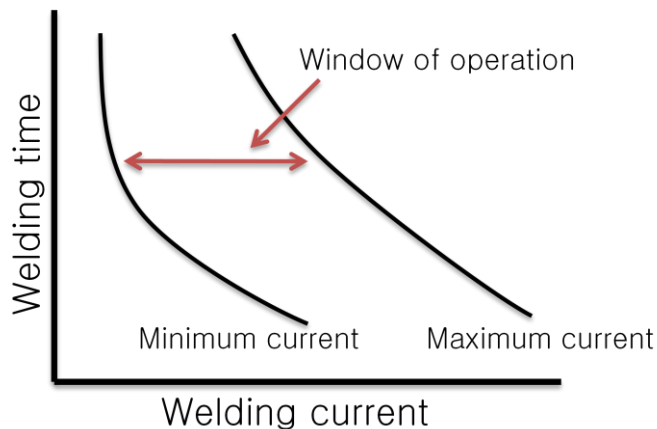
Fig. 2.15 an example of the weld lobe diagram

2.3.3 Weld defects

Spot welds are not free from defects, which can be largely categorized into two groups; external and internal discontinuities [44].

External discontinuities

Defects that appear on the weld surface fall into this category. They usually can be observed by bare eyes or with the aid of low magnifying microscope. The prevention of external defects in most cases comes from the adjustment of welding parameters [44].
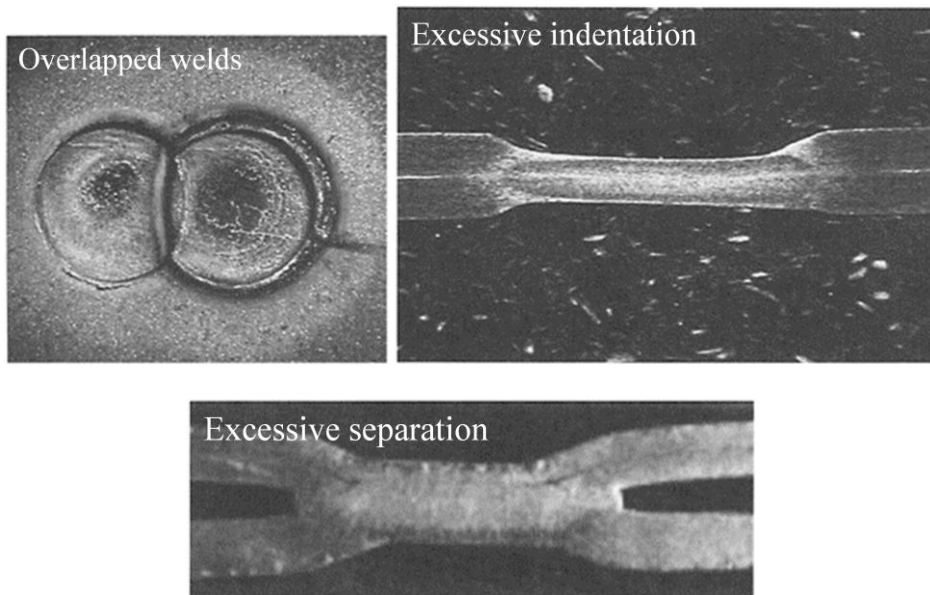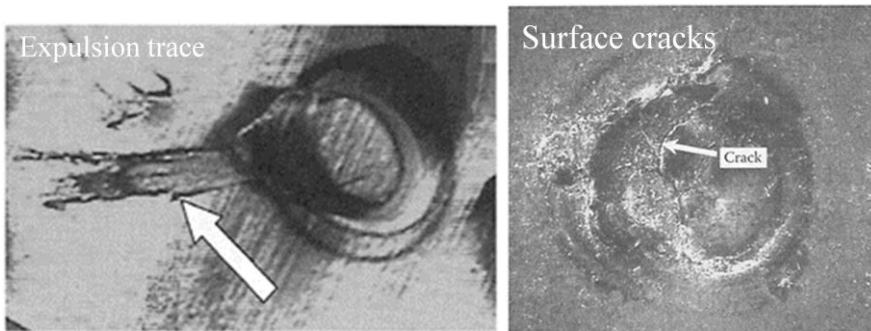
Fig 2.16 several examples of external discontinuities in RSW [44]

Internal discontinuities

Internal discontinuities are found inside of the welds and revealed only by means of metallographic examination of weld cross sections or non-destructive tests. Like in Fig. 2.17, gaseous bubbles from the fusion stage, as the nugget solidifies, leads to porosity due to solidification shrinkage. This does not however pose a threat as long as such voids confined in the center of the nugget because it is at the heat affected zone where the most strain is concentrated [44, 46].
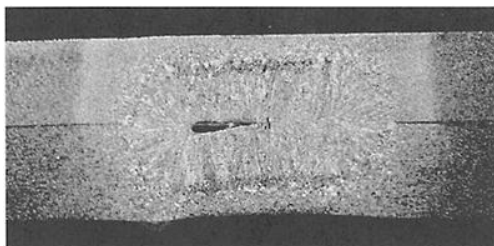
Fig. 2.17 a large void in a mild steel weld [44]
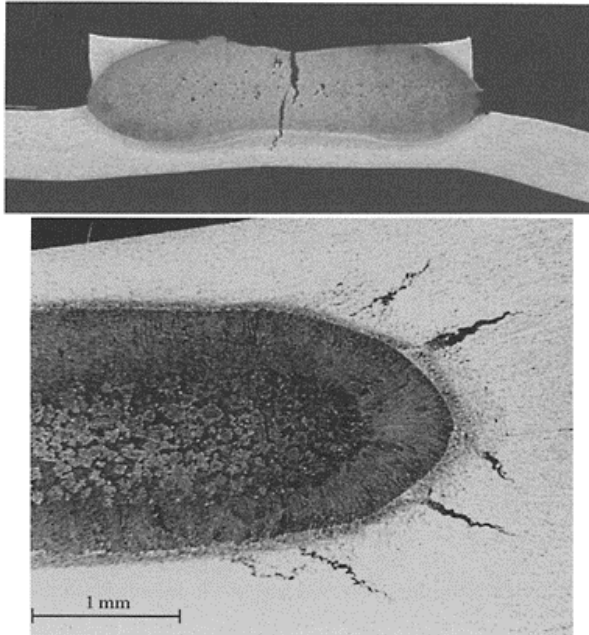
Fig. 2. 18 weld cracks in AA6111 (upper) and AA5754 (lower) [44]

Weld cracks can also be found in spot welded materials. Fig. 2.18 shows weld cracks in aluminium spot welding. Various remedies for weld crack in aluminium alloy have been tested by Hongyan et al. [47]. Mechanical means to suppress weld crack are experimented; for example, flat electrode types are better than domed ones in suppression of weld crack [47].

2.4 Spot weldability of high strength steels

2.4.1 Suitable weld condition

The lobe curve diagrams are a useful tool to see suitable welding conditions of

certain materials. Since a larger process window allows flexibility during the production process, a broad range between the minimum and maximum weld current is appreciated in industry. It is known that highly alloyed steel needs less current to than low-alloy steel [48]. A comparison of weld lobe curves of mild steel and IF (interstitial free) steel is illustrated in Fig. 2.19; the latter is hardly alloyed and hence requires more current value. The addition of alloying elements in steel increases its bulk resistance, so that heat generated from welding process increases [11]. Therefore, for an IF steel to acquire the same nugget size as mild steel, it requires the current to be maintained for a longer period. Fig. 2.20 is the weld nugget growth graph for three different steel alloys. The more alloyed steel, 590TRIP steel, has the suitable weld current range that is overall lower than other alloys by the same principle.
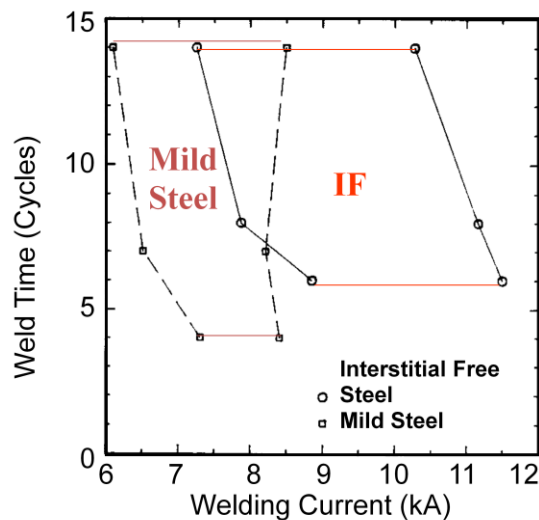
Fig. 2.19 weld lobe curves for mild steel and IF steel [48]
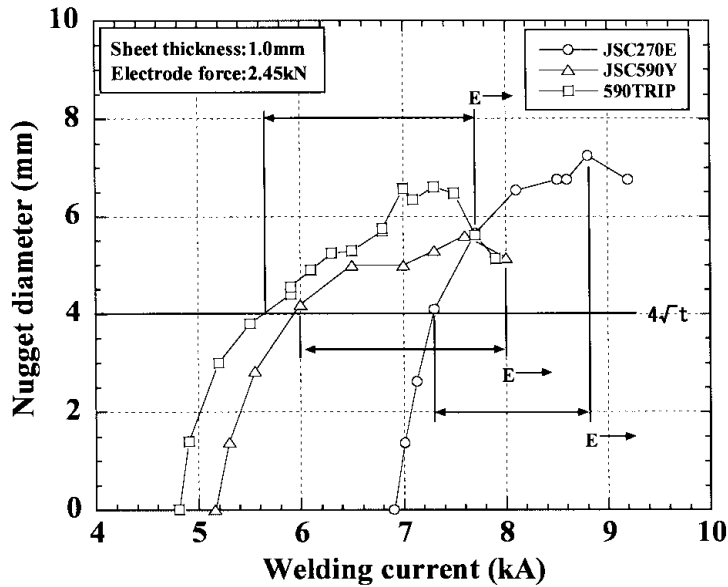
Fig. 2.20 effect of weld current on nugget diameter [13]

2.4.2 Carbon equivalent

In typical resistance spot weld process, cooling rate is very rapid ranging from 1,000-10,000 K s^{-1} because of the quenching effect from the copper electrodes [49, 50]. As a result, martensite forms at the fusion zone, increasing hardness around weld compared with the base metal. When considering weldability, the carbon equivalent is important because it is closely related to hardenability around the weld zone. Typically, highly alloyed steels have the high value of carbon equivalent. Many different empirical equations have been published for determining carbon equivalent [13, 51, 52], of which are listed below.

$$\text{Ceq(wt\%)} = C + \frac{Mn}{6} + \frac{Cu + Ni}{15} + \frac{Cr + Mo + V}{5} \qquad (2.3.3)$$

$$\text{Ceq(wt\%)} = C + \frac{Mn}{6} + \frac{Cu + Ni}{15} + \frac{Cr + Mo + V}{5} \qquad (2.3.4)$$

$$\text{Ceq(wt\%)} = C + \frac{Mn}{6} + \frac{Si}{24} + \frac{Ni}{40} + \frac{Cr}{5} \qquad (2.3.5)$$

2.4.3 Weld strength test

Weld strength from spot welded part needs to be evaluated to ascertain the appropriate integration of steels into automobile production. According to Japanese standards [53, 54], two types of tensile testing methods are employed to assess weld strength, and they are shown schematically in Fig. 2.21. For shear tensile stress test, TSS in short, machined materials are spot welded at one end and horizontally dragged until failure. Samples spot welded into a cross-shaped piece and then pulled apart normal to the plate plane involve a cross tensile strength test, CTS in short. In both cases, the fracture tensile strength is measured [53, 54].

28
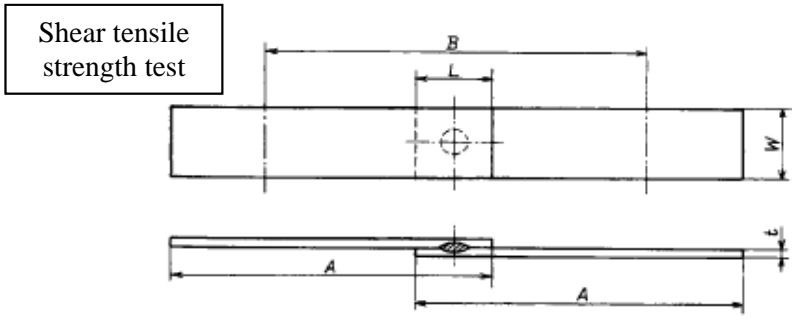
W=30, L=30, A=100, B=70 (mm)
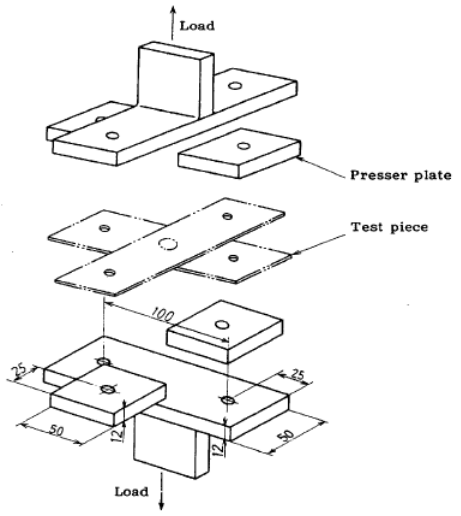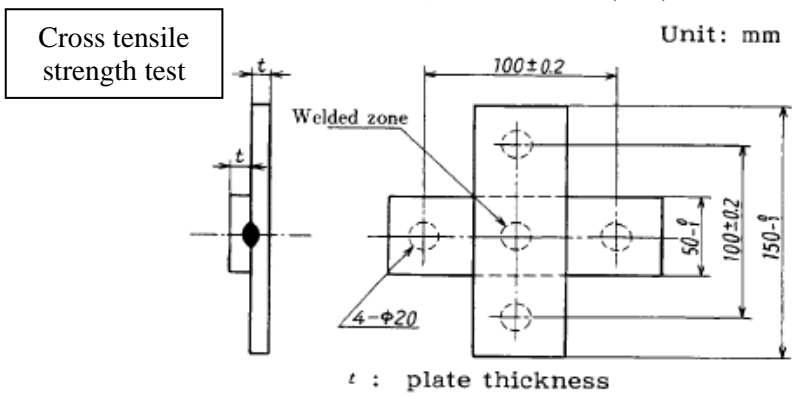
Fig. 2.21 specimen dimensions and shapes for shear tensile and cross tensile tests [53, 54]

The shape of the weld fracture surface determines the fracture mode of weld failure (Fig. 2.22). Plug fracture usually means the part was welded well and strong enough to withstand the load because it fails around the nugget. If fracture occurs in a partial plug fracture mode, it is not as good as the plug fractured case, but is tolerable. Lastly, interfacial fracture is the case where weld nugget is not strong at all. It happens with insufficient nugget size. Interfacial fracture mode should be avoided, and plug fracture mode is ideal [9].

The weld nugget size is a critical factor for weld strength [13]. In the upper graph in Fig. 2.23, shear strength increases in accordance with nugget size. The lower graph in Fig. 2.23 shows the relations between base metal strength and TSS, CTS. While TSS increases with base metal strength, CTS decreases after peaking at the point where the base metal strength is 590MPa. This is explained by the fact carbon equivalent of high strength steel usually is higher [14].

Plug fracture mode

Partial plug fracture mode

Interfacial fracture mode

Sheared fracture nugget

Corona
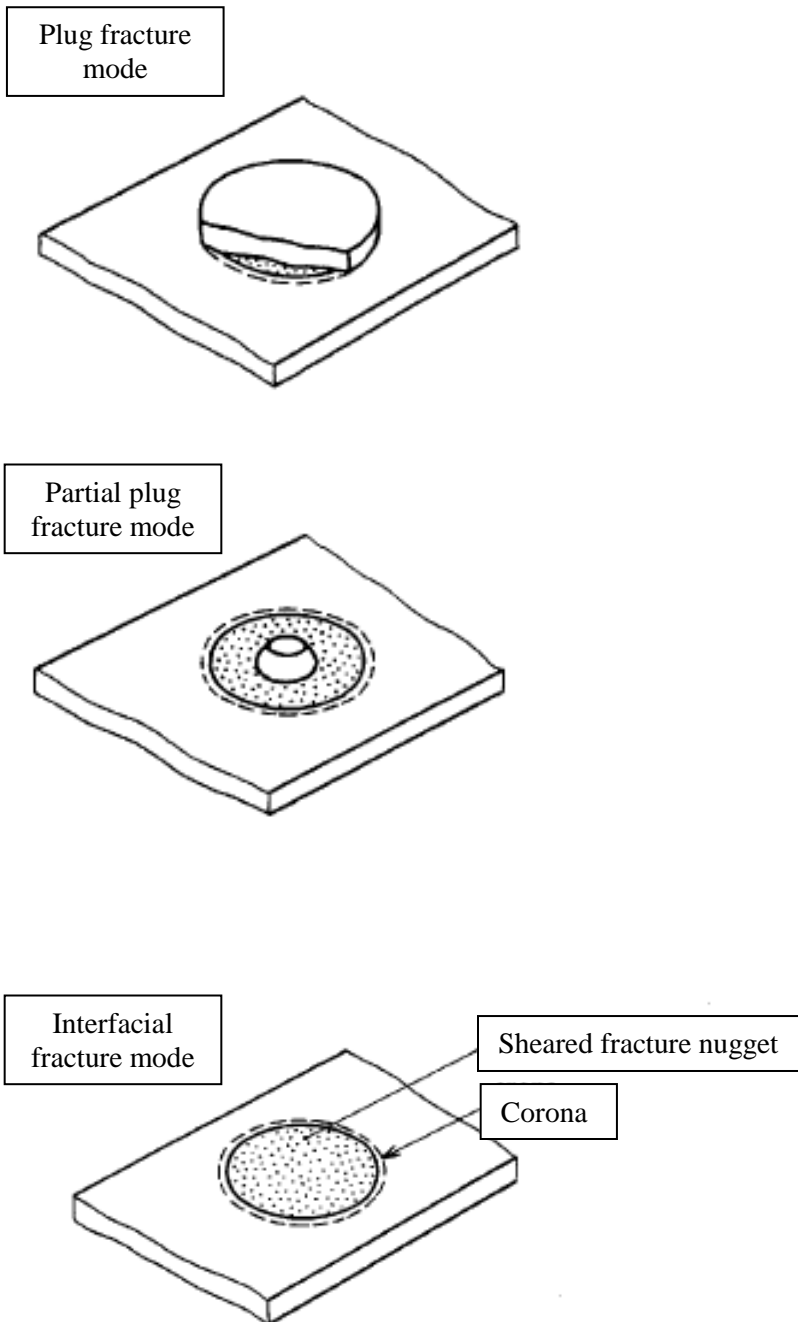
Fig. 2.22 different weld fracture mode; plug fracture, partial plug fracture and interfacial fracture mode [53, 54]
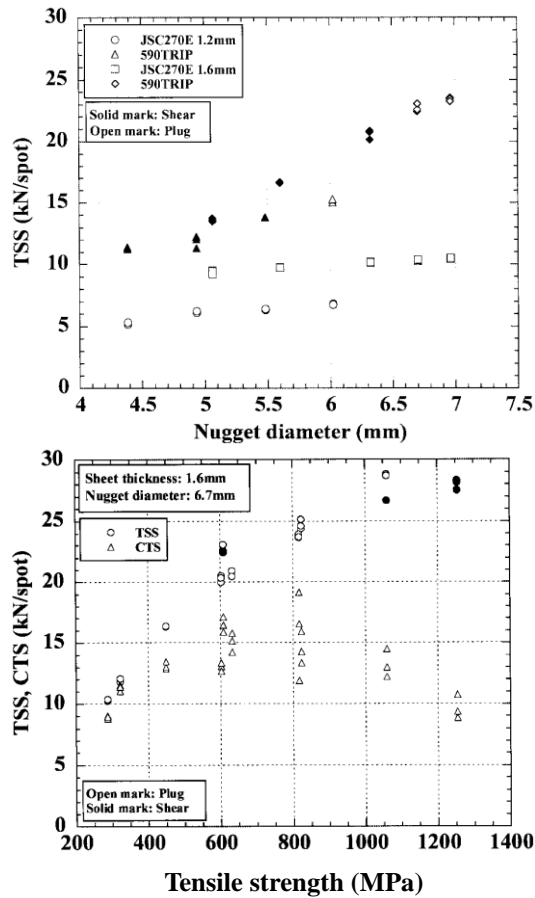
Fig. 2.23 effect of nugget diameter(upper) and base metal strength(lower) on TSS and CTS of joints [13]

Another important factor when assessing spot weldability is ductilitiy ratio, which is expressed as CTS/TSS value. While the origin of it remains unclear, it is known that a weld with a ductility ratio more than 0.5 shows better toughness [55]. Thus, it is imperative to acquire a reasonable ductility ratio to avoid weld embrittlement problem for automotive steels.

3 Experiments

3.1 Material specification

 Table 3.1 specifies the compositions of 4 similar alloy systems that were investigated for this work. Alloy designs were conducted based on the former δ-TRIP steel compositions [6-8, 10]. Carbon and aluminium contents were purposely varied in order to see their effect on δ-ferrite stability.

Table 3.1 composition of investigated alloys

Alloy	C (wt%)	Mn (wt%)	Si (wt%)	Al (wt%)
3LA	**0.30**	0.52	0.20	**3.50**
3HA	**0.30**	0.51	0.21	**5.60**
4LA	**0.40**	0.51	0.19	**3.50**
4HA	**0.40**	0.50	0.18	**5.60**

 Fig. 3.1 shows the calculated equilibrium phase diagrams for each alloy using commercial thermodynamic simulation software, ThermoCalc with the TCFE6 database. Predictions can be made from the equilibrium phase diagrams that the δ-ferrite that forms in the early stages of solidification would not completely disappear except in the case of 4LA. Considering remaining fraction of δ-ferrite at room temperature, the stability of δ-ferrite in 3HA is the highest, and then decreases in the order 3LA, 4HA and 4LA.
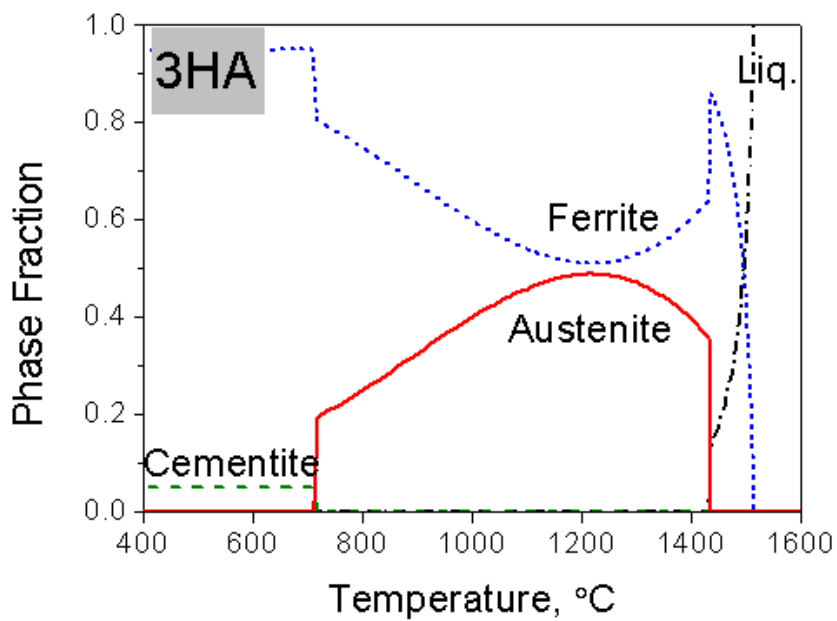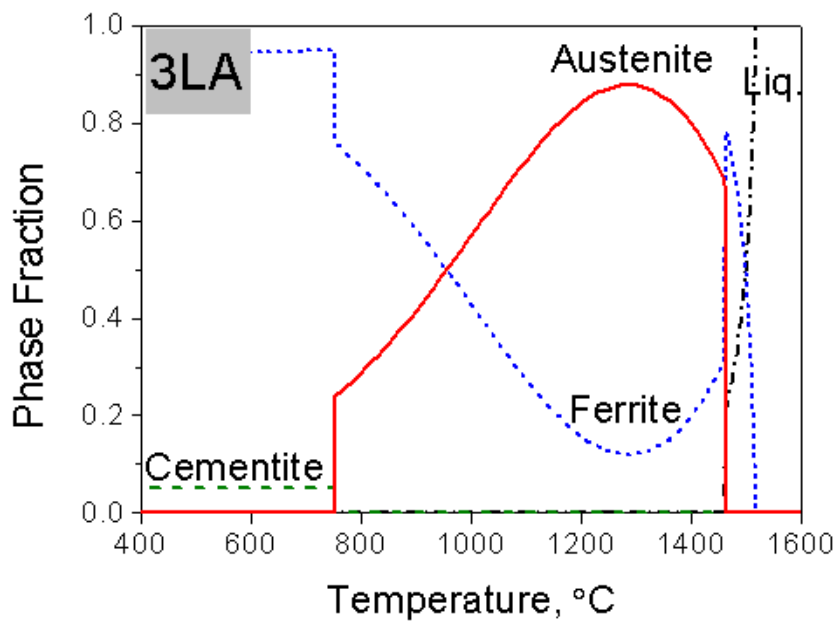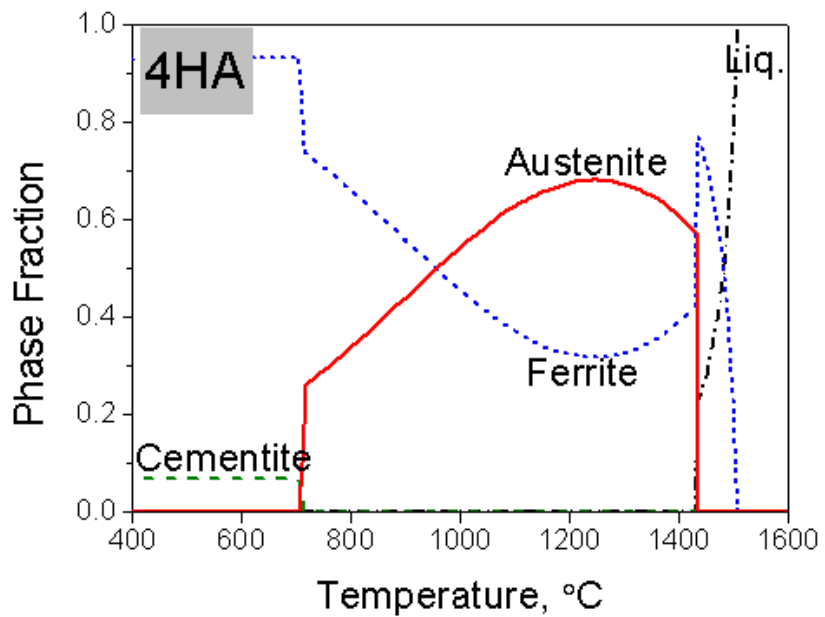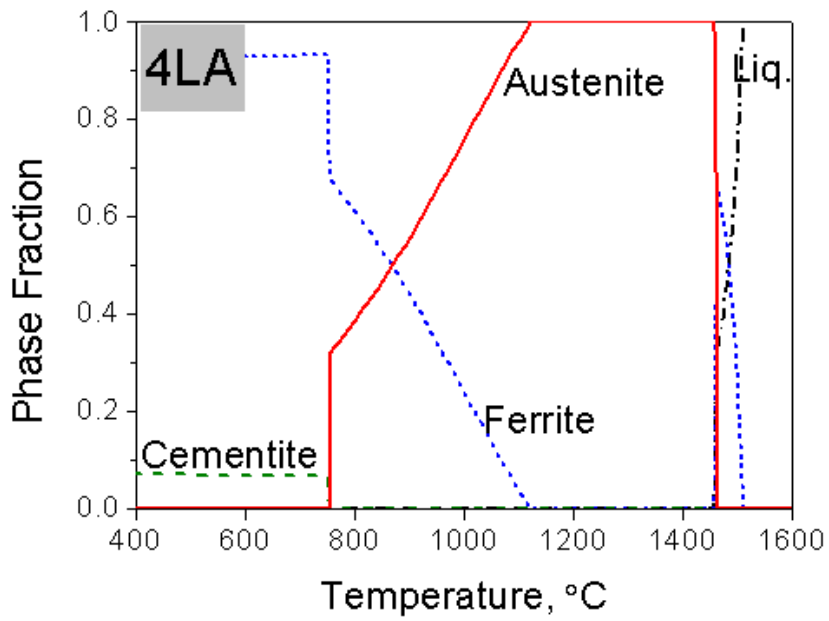
Fig. 3.1 equilibrium phase diagrams for 3LA, 3HA, 4LA and 4HA alloys

Specimens were produced as vacuum-melted ingots of 25 kg and austenitized at 1200℃ for 1 h followed by hot-rolling to 4.5 mm in thickness, with the finishing rolling temperature at above 950℃. After the hot rolling process, the sheets were cold-rolled to a final thickness of 1.2 mm. Images of the microstructure of the hot-rolled specimens are provided in Fig. 3.2.
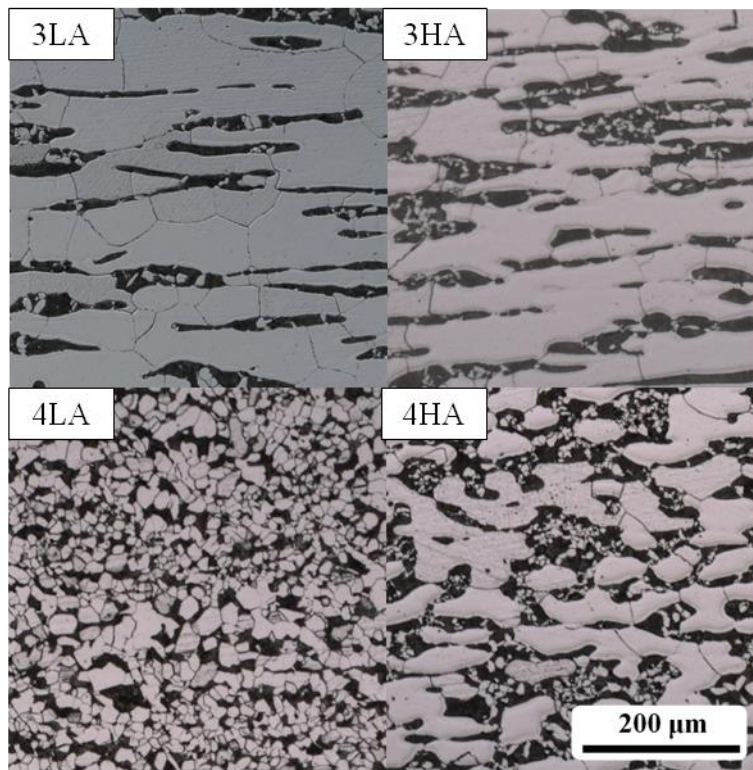
Fig. 3. 2 microstructures of hot-rolled alloys

As expected from the equilibrium phase diagrams, coarse δ-ferrite bands are observed in 3LA, 3HA and 4HA. Ferrite bands are absent in 4LA because of the

low stability of δ-ferrite. It is suggested that δ-ferrite transformed entirely into austenite at the high hot-deformation temperatures, and the formation of polygonal ferrite occurred instead on cooling following solidification.

3.2 Pre-welding test

3.2.1 Heat treatment cycle

Since the alloys will not be used as-cold-rolled condition, proper heat treatment needs be planned to optimize mechanical properties before moving on to weldabilty tests. On designing the heat treatment cycle, two variations, intercritical annealing temperature and isothermal transformation (austempering, hereafter) time were set. For intercritical annealing, the temperatures were changed from 780℃ to 840℃ with an increment of 20℃. The austemepring temperature was set to be 400℃, though durations for it varied from 30 s, 60 s, 120 s, 300 s to 600 s. Such variations were made based on previous research on δ-TRIP steels [5-10]. A brief illustration of heat treatment design is presented in Fig. 3.3.
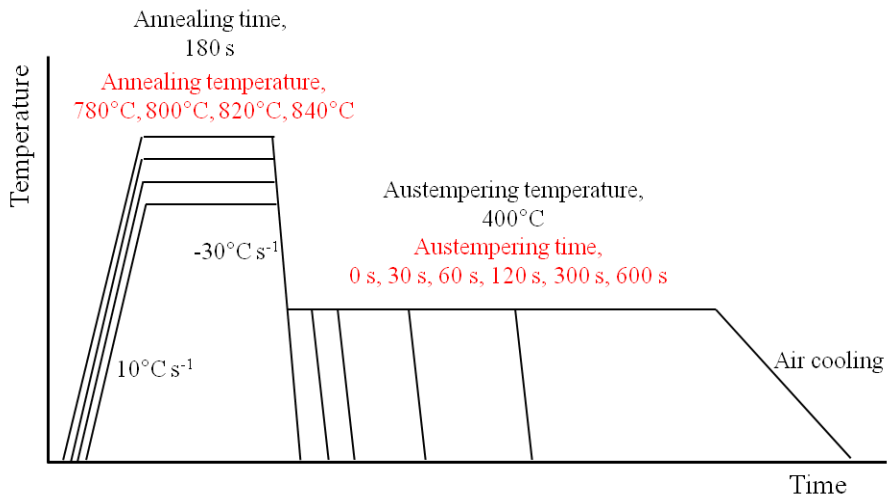
Fig. 3.3 heat treatment cycles for new alloys

3.2.2 Metallography

Heat treated samples were prepared with conventional method for metallographical study. Mechanically polished surfaces were etched with 2% nital etchant, and the microstructures were revealed using optical microscopy (Eclipse MA200, Nikon) and scanning electron microscopy (FE-SEM, Carl Zeiss Ultra 55).

3.2.3 Mechanical tests

The mechanical properties of heat treated samples were assessed using a tensile testing machine (Zwick/Roell Z100). Heat treated samples were machined to the dimensions for tensile tests according to standard practice [56]. Fig. 3.4 shows the shape and the dimensions of the tensile test sample used.
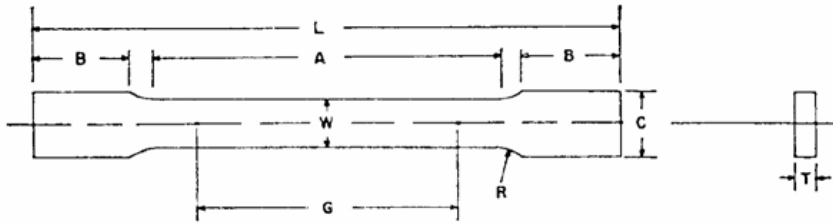
G=25, W=6.25, T=thickness of material, L=100, A=32, B=32, c=10, R=6(mm)

Fig. 3.4 rectangular tension test specimen [56]

The fraction of retained austenite is affected by heat treatment conditions since its stability is achieved by carbon enrichment during the bainitic transforming period. The fraction of retained austenite was measured using X-ray diffraction (Bruker D8 Advance), and by using scanning electron microscopy with electron back scattered diffraction.

3.3 Spot welding tests

3.3.1 Welding conditions

For the evaluation of weldability, spot welding of fully heat treated samples was conducted according to the conventional standard [57, 58]. First, samples were spot welded with single phase AC spot welder (75 kVA) with maximum electrode force of 7 kN (pneumatic). Direct current spot welding was also conducted using inverter DC spot welder (200 kVA) with maximum electrode force of 20 kN (servo-motor powered). The welding conditions for each process are shown in Table 3.2. Weld conditions were in fact identical; weld times are differently

39

written because of the difference in units.

Table 3.2 spot welding conditions (upper: single phase AC spot weld, lower: inverter DC spot weld)

Force	Welding time / cycle, 60 Hz				Electrode		
	Squeeze	Weld	Hold	Metal	Type	Tip dia.	Coolant
4.0 kN	40	17	17	Cu-Cr	DR	6.0 mm	41 /min

Force	Welding time / ms				Electrode		
	Squeeze	Weld	Hold	Metal	Type	Tip dia.	Coolant
4.0 kN	646	272	272	Cu-Cr	DR	6.0 mm	41 /min

3.3.2 Weld microstructure

Spot welded specimens were sectioned in half and weld microstructures were revealed using the same method as described earlier in 3.2.2. The formation of δ-ferrite in the weld zone was studied. The size of each weld nugget was determined by measuring the nugget diameter (Fig. 3.5). Based on measurements of nugget size, lobe diagrams for each alloy were acquired.
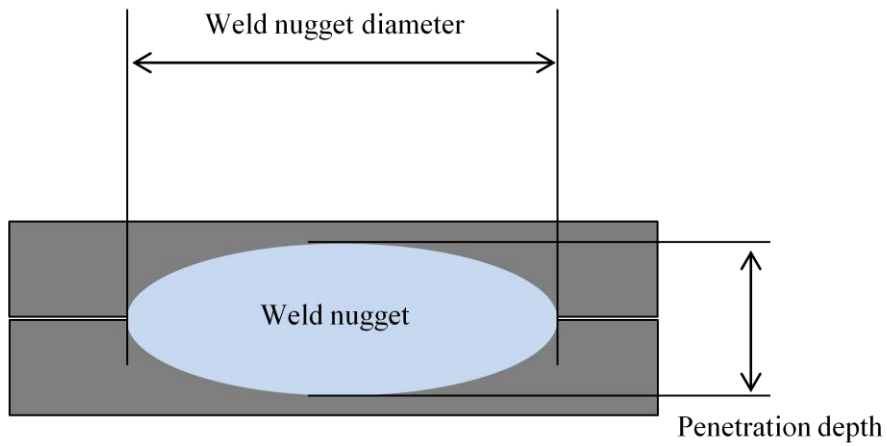
Fig. 3.5 definition of nugget size [53, 54]

3.3.3 Weld property tests

Weld strength was evaluated by shear tensile strength test, TSS test, and cross tensile strength test, CTS test. Specimens were heat treated and machined according to a Japanese industrial standard [53, 54]. The ductility ratio was determined as CTS/TSS. The hardness distribution around weld nugget was measured using Vickers hardness tester, Mitutoyo HR-522.

4 Pre-welding tests

4.1 Microstructure

Microstructures obtained from annealing and quenching processes are illustrated in Fig. 4.1. Specimens were intercritically annealed at 840℃ for 3 min before being water quenched to ambient temperature.
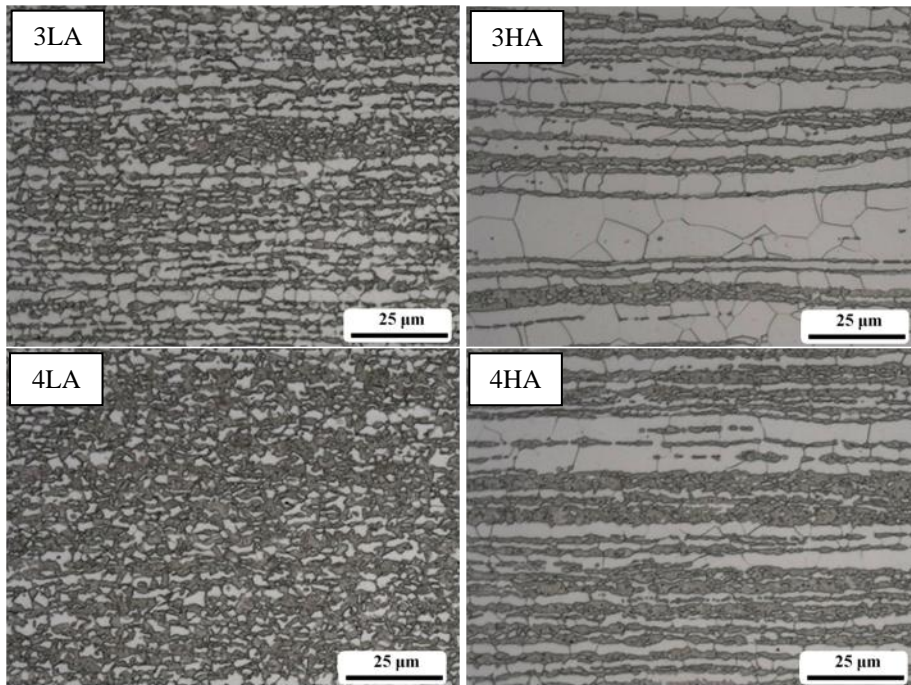
Fig. 4.1 microstructures of quenched specimens after 840℃ annealing for 3 min

Similar microstructures for hot-rolled conditions in Fig. 3.2 can be observed. However, the substitution of pearlite due to rapid cooling by martensite is worth

noticing, as shown in Fig. 4.2. Microstructure of Alloy 4LA can be characterized as rather homogenous, while the other alloys clearly show coarse δ-ferrite bands.
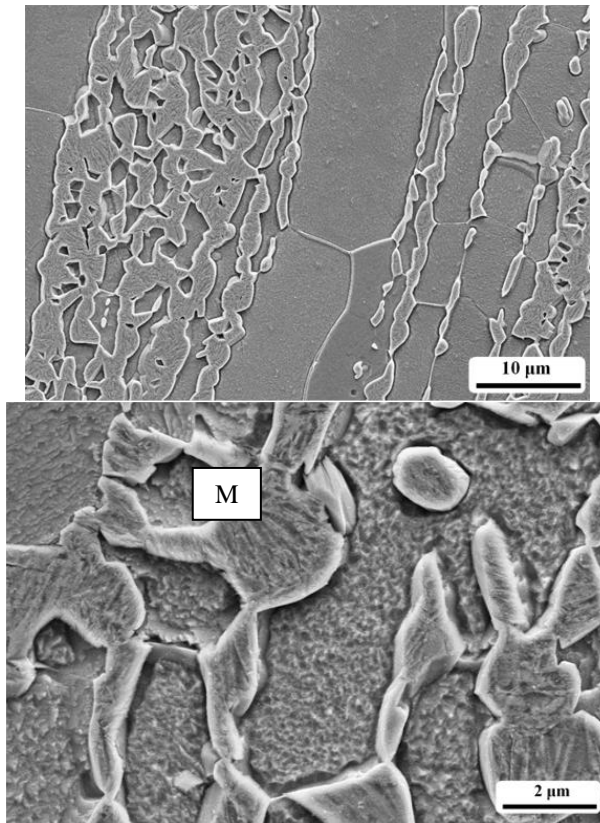
Fig. 4.2 SEM image of quenched 4HA revealing martensite in the matrix
(M : martensite)

To see the effect of annealing temperature, alloys were annealed at different temperatures, 780℃, 800℃, 820℃ and 840℃. Their respective microstructures are seen in Fig. 4.3. Each specimen was annealed for 3 min with different

temperatures followed by austempering at 400℃ for 10 min.

3HA annealed at 820℃

3HA annealed at 840℃

15 µm

15 µm

4LA annealed at 780℃

4LA annealed at 800℃

15 µm

15 µm

4LA annealed at 820℃

4LA annealed at 840℃

15 µm

15 µm

4HA annealed at 780℃

4HA annealed at 800℃

15 µm

15 µm
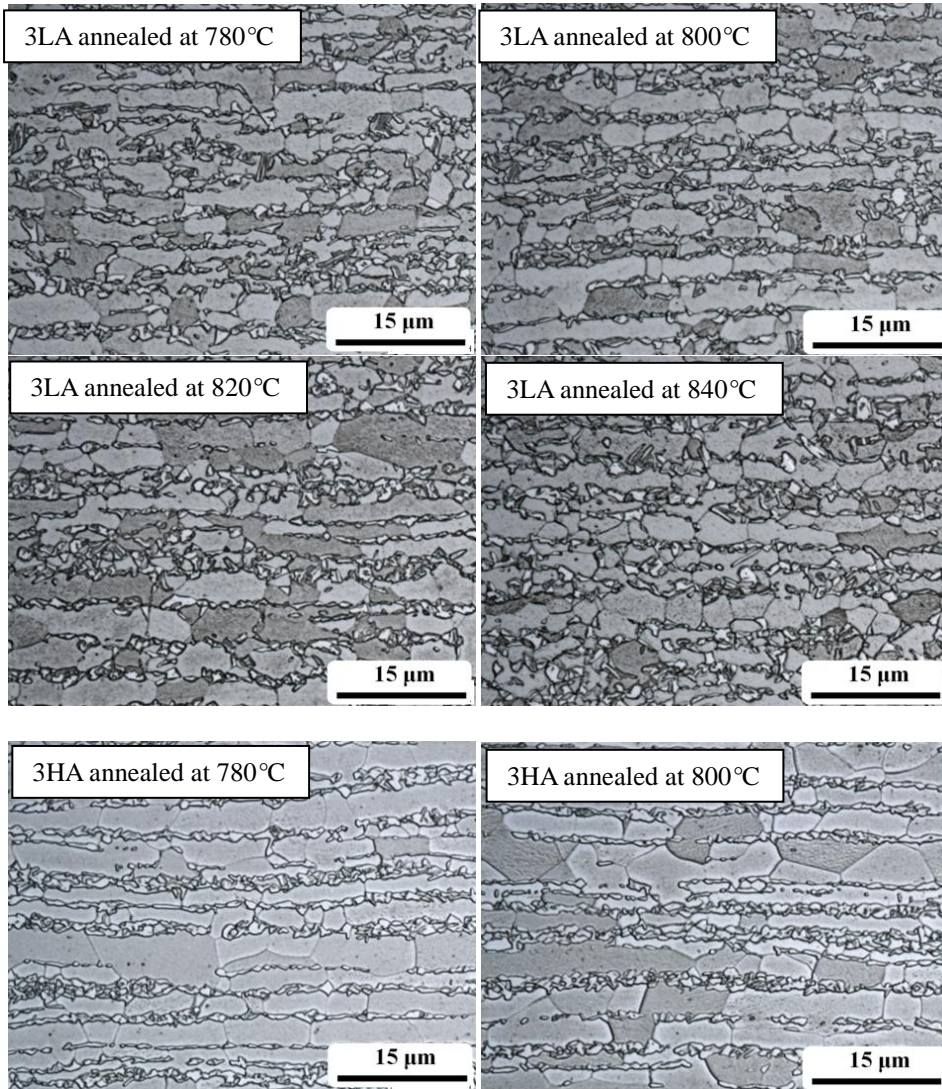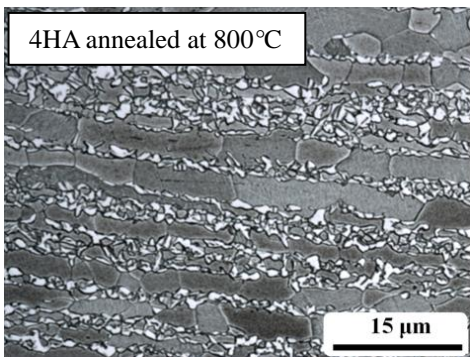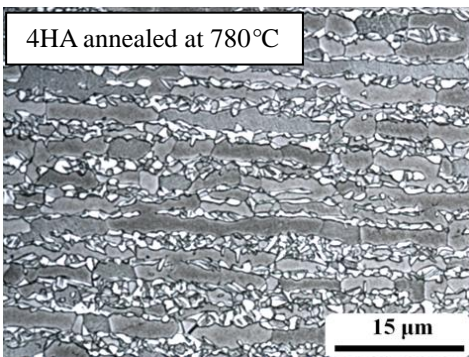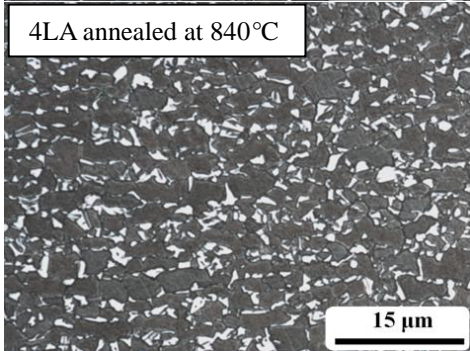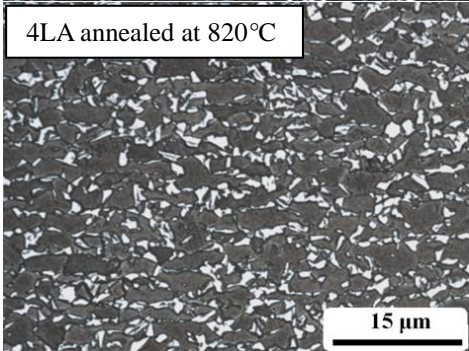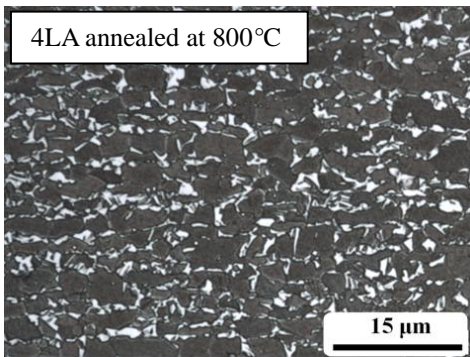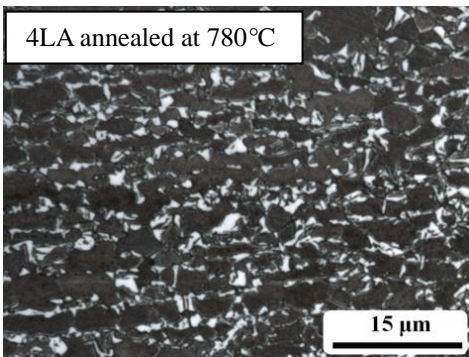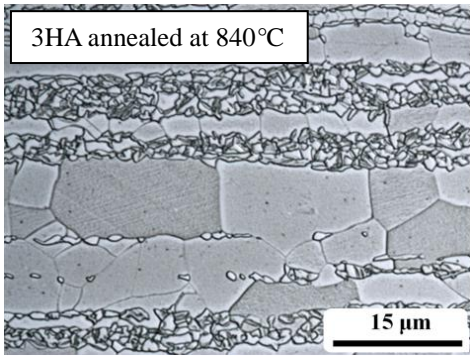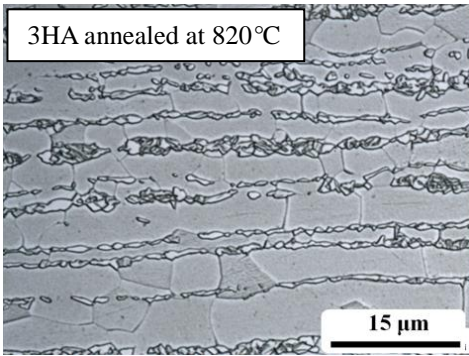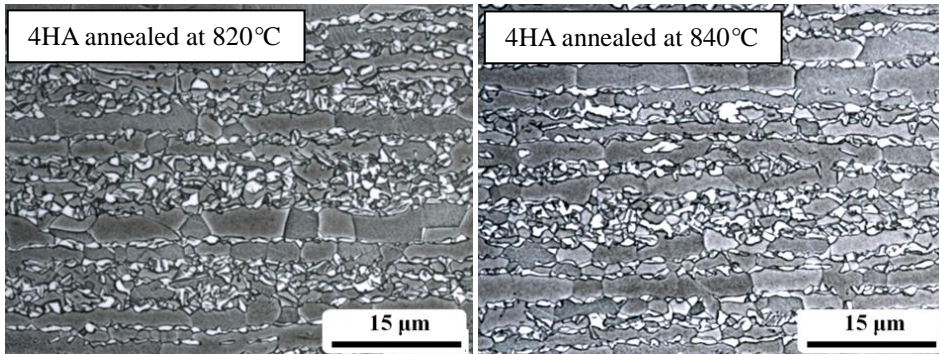
Fig. 4.3 microstructures after annealing with temperature variation

The annealing temperature, over the range studied, does not seem to have a significant effect on microstructure. As expected from the equilibrium phase diagrams, except for 4LA, δ-ferrite bands are retained in the microstructures. In between the δ-ferrite are fine mixtures of retained austenite and bainite that formed during austempering.

The formation of austenite was studied using EBSD analysis as shown in Fig. 4.4. Specimens were annealed at 840℃ for 3 min and austempered at 400℃ for 10 min. In between δ-ferrite bands, some austenite stabilized due to carbon enrichment has survived after the whole heat treatment. Such retained austenite contributes to good mechanical properties by transforming into martensite on loading.

46

3LA

3HA

4LA
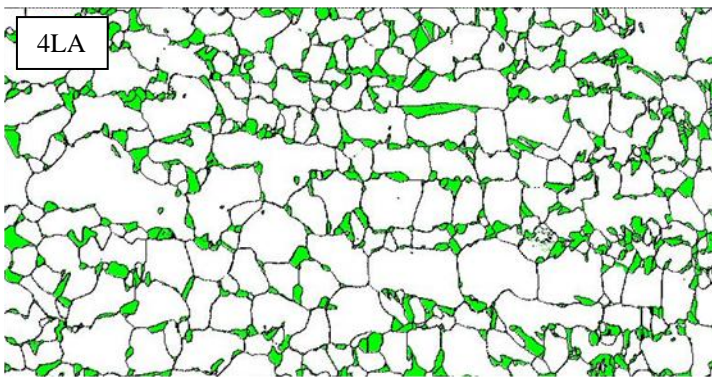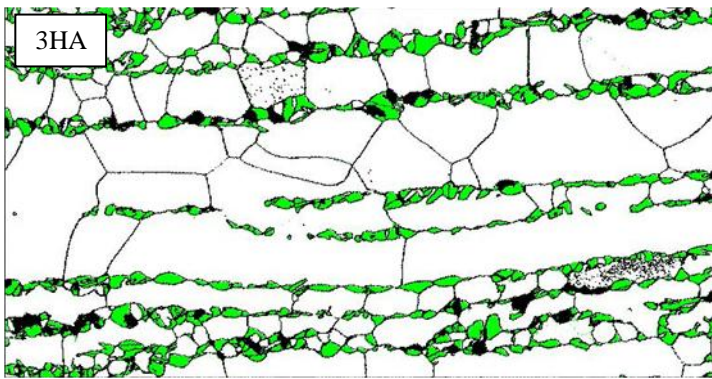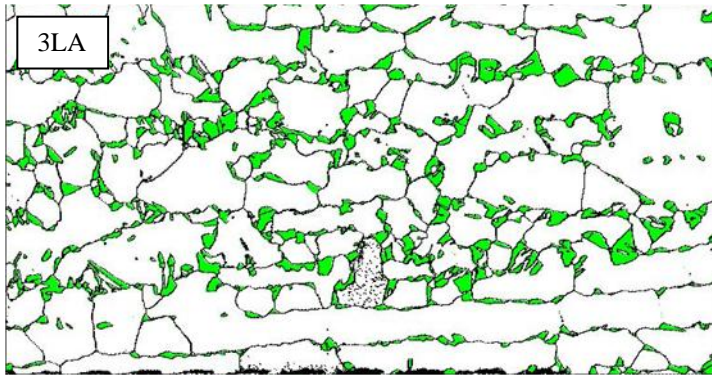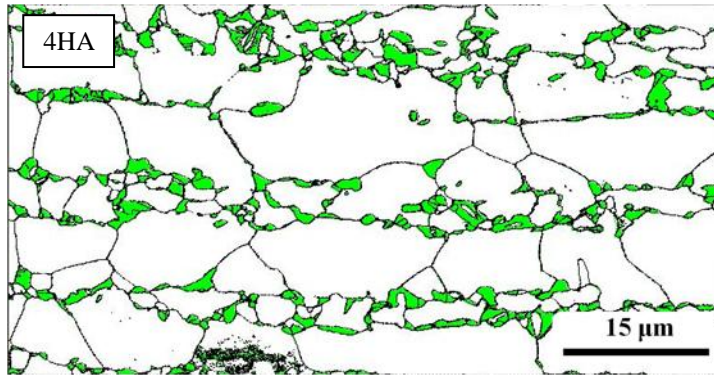
Fig. 4.4 EBSD images of alloys after annealing and austempering
(white : ferrite, green : austenite)

Heat treatment trials with different isothermal holding times were conducted to see the effect of austempering duration on microstructural changes. Alloy 3HA was picked and processed with different annealing and austempering times. Coarse δ-ferrite bands are observed along with mixtures of retained austenite and bainite, Fig. 4.5. The grain sizes of retained austenite are roughly 3-4 μm, Fig. 4.6. However, significant changes were not noticed in the microstructures as a function of austempering time.
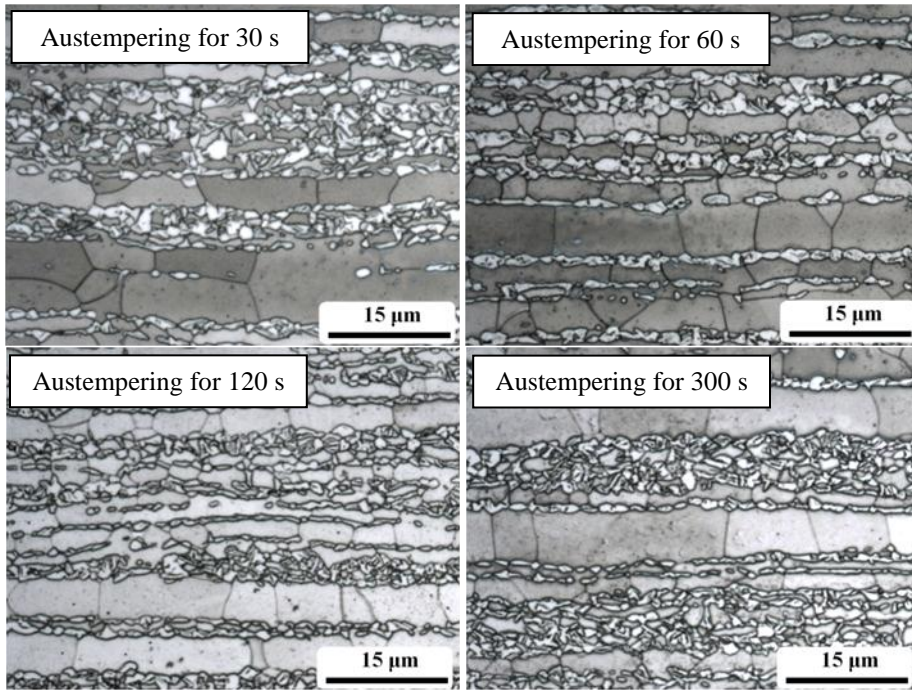
Fig. 4.5 microstructure change in the alloys with austempering time variations

(annealed at 840℃ for 3 min, austempered at 400℃ for different holding times)
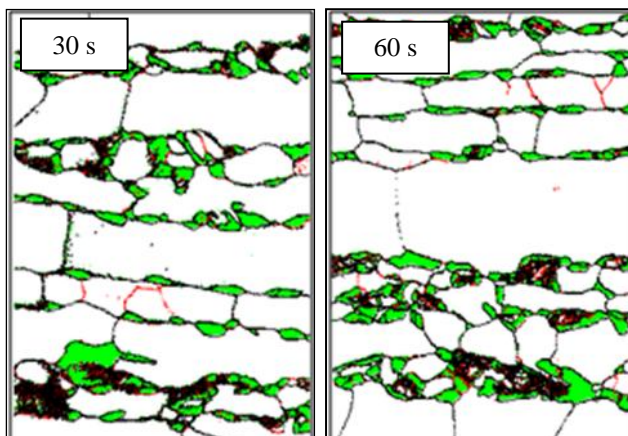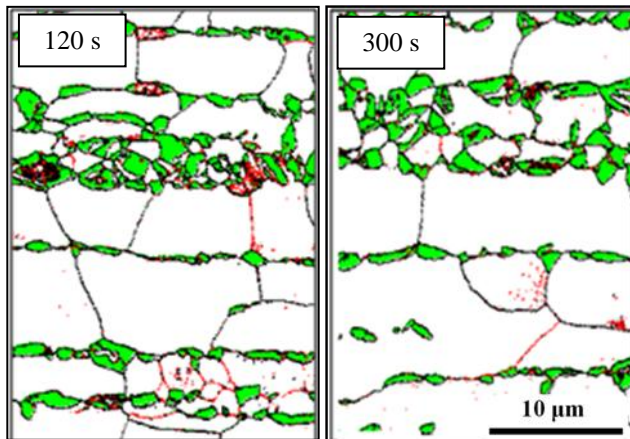
Fig. 4.6 EBSD images of alloy 3HA with different austempering time

(white : ferrite, green : austenite)

EBSD analysis for each case was done and the results are shown in Fig. 4.6. The fraction of retained austenite is similar in each case according to the X-ray diffraction analysis in Fig. 4.7. Around 12% of austenite was retained in the matrix after any heat treatments except for the quenched ones. Longer holding does not seem to have an effect once bainitic transformation was allowed for 30 s. Therefore it can be concluded that most austenite is already stabilized during bainitic transformation at short time.
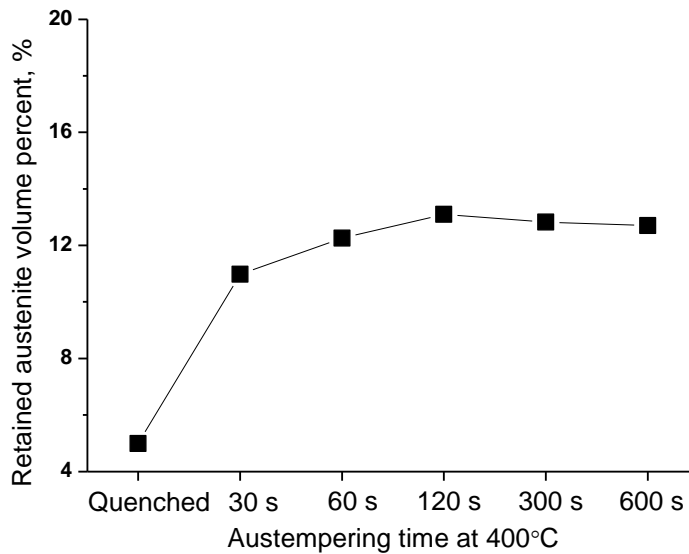
Fig. 4.7 retained austenite volume fraction change with different austempering times

4.2 Mechanical property test

4.2.1 Property dependence on annealing temperatures

Results from tensile tests are shown in Fig. 4.8. Specimens were austemepered at 400℃ for 10 min, but before austempering they were intercritically annealed for different conditions. Annealing times remained the same as before, 3 min, but annealing temperature changed from 780℃ to 860℃. Ultimate tensile strength, UTS, is the measure of strength of steel, and ductility is expressed by total elongation. Judging from the results, the mechanical properties are not particularly sensitive to annealing temperatures.
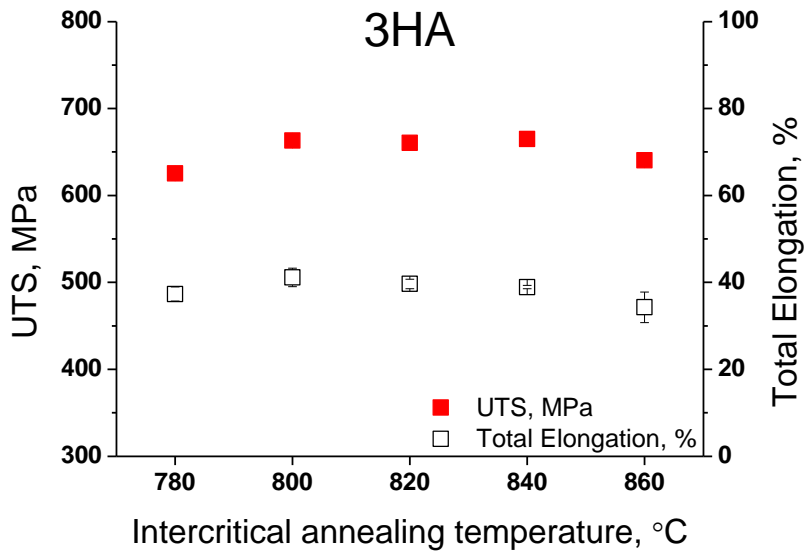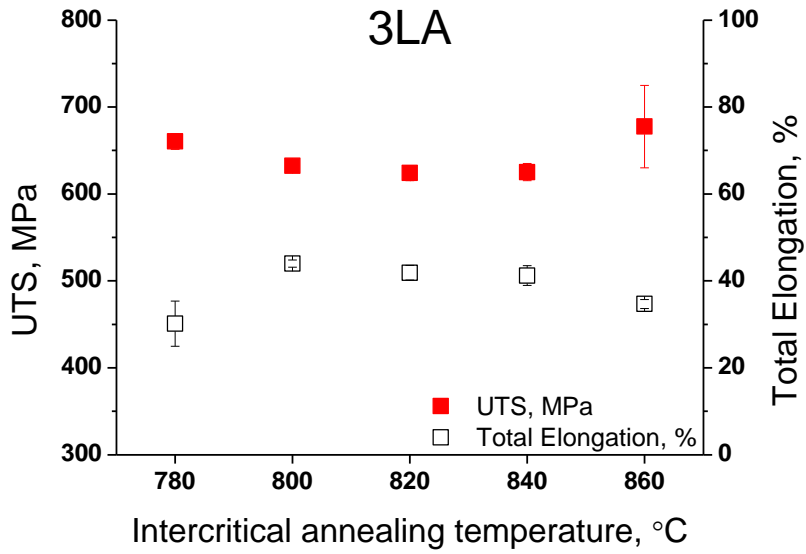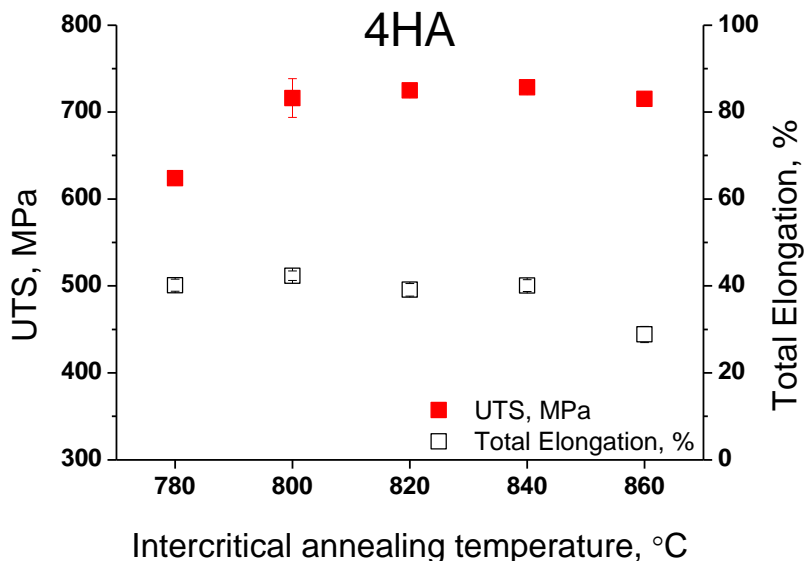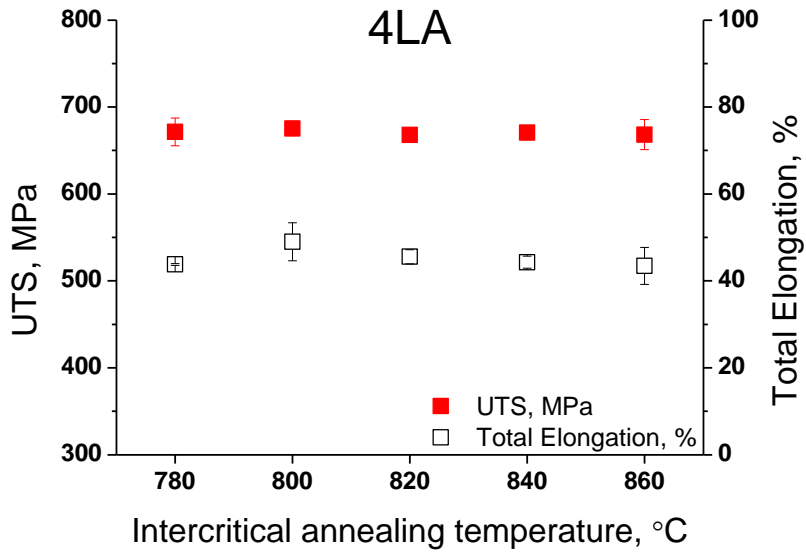
Fig. 4.8 mechanical properties with different annealing times

Table 4.1 mechanical property changes with different annealing times

3LA				
Annealing temperature, ˚C	Yield strength, MPa	UTS, MPa	Uniform elongation, %	Total elongation, %
780	454	660	26	30
800	471	632	33	44
820	472	624	32	42
840	470	625	31	41
860	503	677	26	35

3HA				
Annealing temperature, ˚C	Yield strength, MPa	UTS, MPa	Uniform elongation, %	Total elongation, %
780	451	625	28	37
800	481	663	31	41
820	483	660	30	40
840	486	665	30	39
860	470	640	24	34

4LA				
Annealing temperature, ˚C	Yield strength, MPa	UTS, MPa	Uniform elongation, %	Total elongation, %
780	524	671	34	44
800	525	675	36	49
820	518	668	35	46
840	526	670	34	44
860	515	668	30	43

4HA				
Annealing temperature, ˚C	Yield strength, MPa	UTS, MPa	Uniform elongation, %	Total elongation, %
780	463	624	32	40
800	507	716	34	42
820	512	725	33	39
840	515	728	33	40
860	514	715	22	29

4.2.2 Property dependence on austempering times

Unlike annealing temperatures, austempering time has great influence on alloys' mechanical properties. Property changes of alloy 3HA with different austempering times are presented in Fig. 4.9. For the quenched case without any bainitic transformation period, due to major martensite formation, the steel exhibited very high strength reaching almost 1 GPa though it was brittle. As retained austenite fraction increases, meaning longer austempering, ductility went up at the expense of strength.
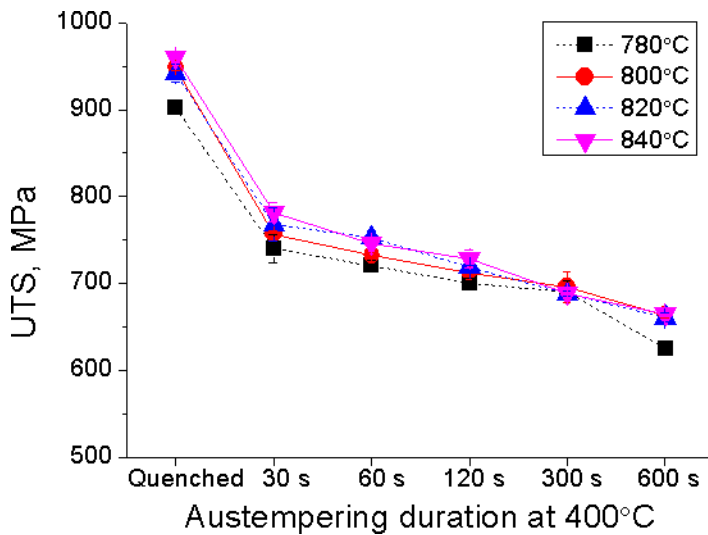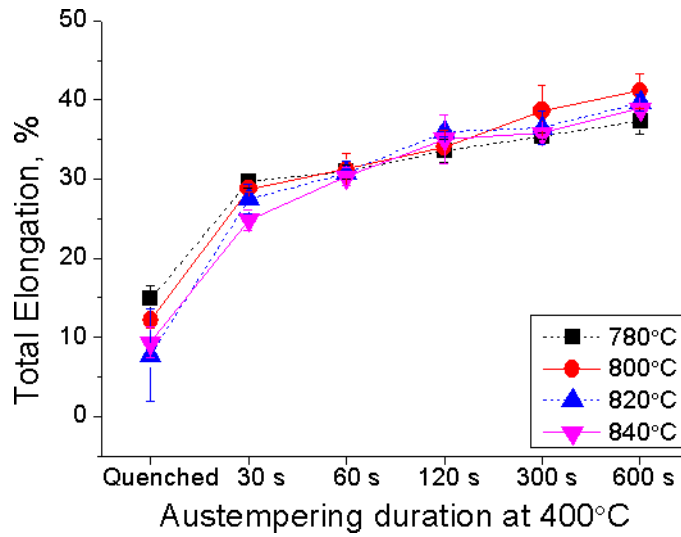
Fig. 4.9 mechanical properties with different austempering times of 3HA

Table 4. 2 mechanical properties of 3HA with different austempering times

Ultimate tensile strength, MPa						
Annealing temperature, ˚C	Austempering time, s					
	0	30	60	120	300	600
780	902	740	720	700	690	625
800	949	757	733	712	696	662
820	942	768	752	718	688	660
840	960	782	746	728	689	665

Total Elongation, %						
Annealing temperature, ˚C	Austempering time, s					
	0	30	60	120	300	600
780	15	30	31	34	35	37
800	12	29	31	34	39	41
820	8	27	31	36	36	40
840	9	25	30	35	36	39

Since attention was placed on the fact that rather short austempering time was already enough to stabilize the austenite, for the sake of high strength, the other alloys, 3LA, 4LA and 4HA, were all tensile tested again after short austempering, 30 s, and results are compared in Fig. 4.10. As predicted, shorter austempering gave better strength with a loss of ductility.
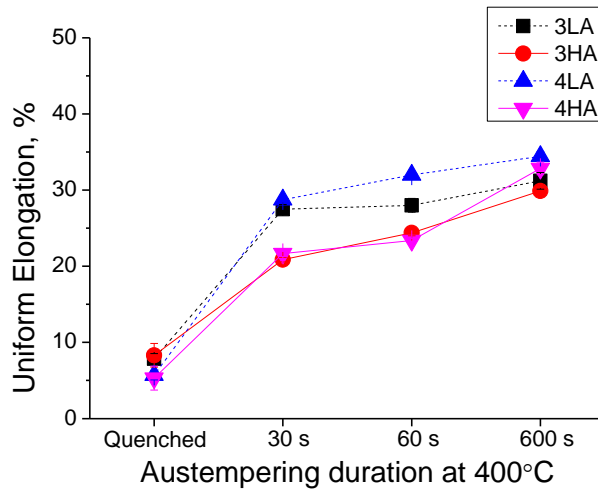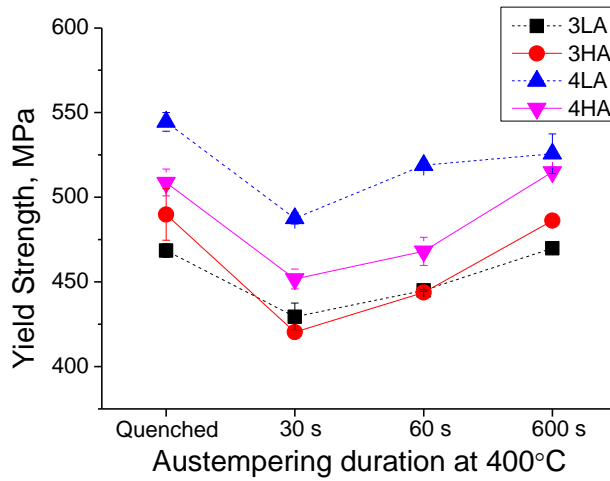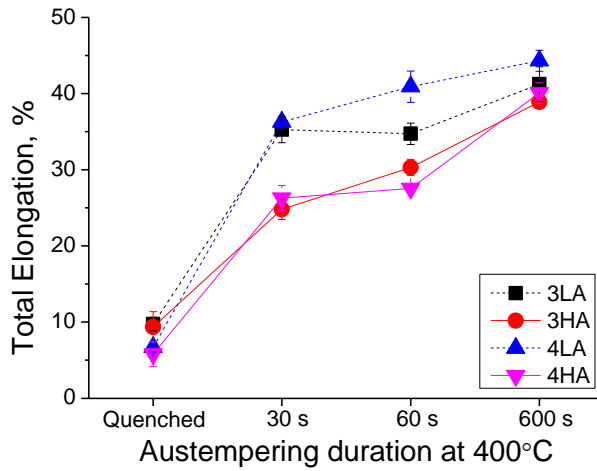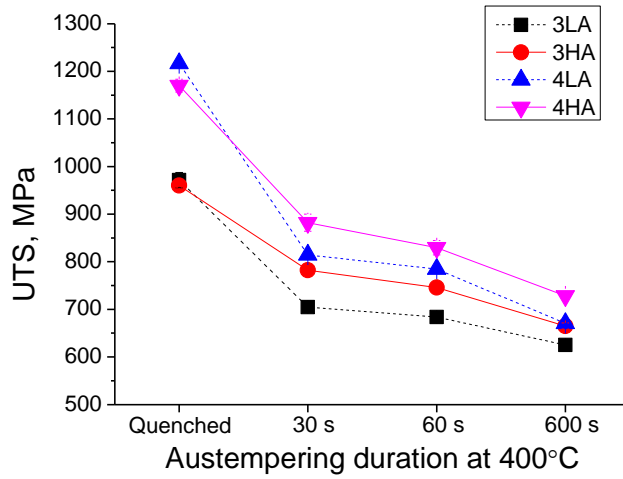
Fig. 4.10 tensile properties for every alloy annealed at 840℃ for 3 min with different austempering conditions

Especially for 4LA and 4HA, tensile strength of more than 800 MPa could be achieved with total elongation of 25% for 30 s of austempering. Tensile strength

of 300 MPa was reduced after austempering for 30 s compared with the quenched specimen. However, the rate of strength reduction was not high after 30 s of austempering, and it is because at first 30 s bainitic transformation occurred rapidly, and after the initial stage transformation rate decreased.

The effect of aluminium on ductility was recognized because 3LA and 4LA showed superior ductility than 3HA and 4HA. It implies that the aluminium that is contained in ferrite matrix may have brought about a deterioration of ductility.

5 Evaluation of spot weldability

5.1 Weld nugget growth

The weld nugget grows in proportional with welding current in both AC and DC spot weld, Fig. 5.1. Sample 3LA, having the least alloying element concentration, showed the widest tolerance for weld condition, without any expulsion observed during AC spot welding. As the solute concentration increases, the suitable weld range seems to narrow down because of the early emergence of expulsion. As discussed earlier, expulsion is a weld defect to be avoided.

WS_{min} is the abbreviation for minimum weld nugget size, and in this work a conventionally recommended criterion for automotive steels [59], $4t^{0.5}$, is used where t is the metal sheet thickness in mm. Weld nugget should exceed WS_{min} in diameter because a small nugget would not be strong enough and is likely to fail in the interfacial fracture mode [59, 60]

Based on acquired weld nugget images, nugget sizes were measured, and the weld currents for expulsion identified. With these, weld lobe curve diagrams for each specimen were drawn as shown in Fig. 5.2, and the effect of two types of weld current compared.

(a) AC welded 3LA   **(b) AC welded 3HA**

I=4.6 kA | 2 mm
I=5.2 kA | 2 mm
I=6.0 kA | 2 mm
I=6.8 kA | 2 mm
I=7.2 kA | 2 mm
I=7.5 kA | 2 mm

I=4.6 kA | 2 mm
I=5.2 kA | 2 mm
I=6.0 kA | 2 mm
I=6.8 kA | 2 mm
I=7.2 kA | 2 mm
I=7.5 kA | (Expulsion) | 2 mm
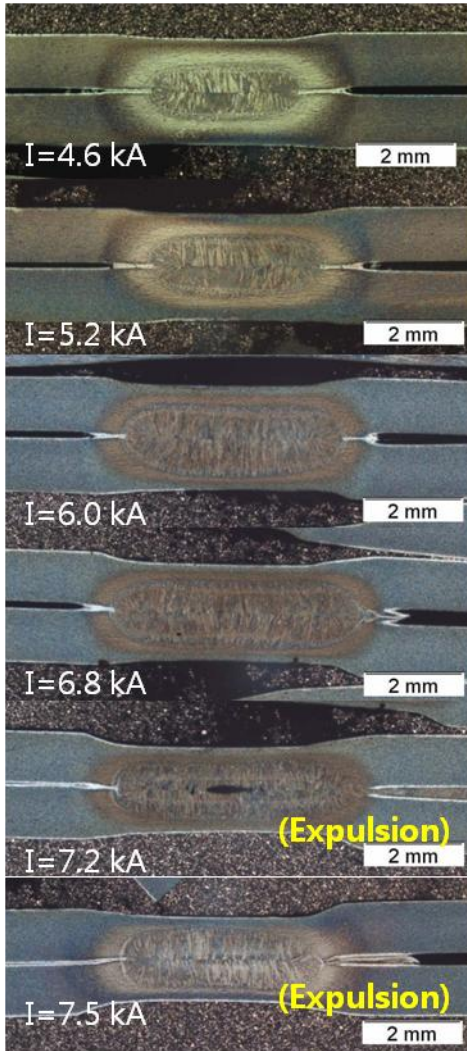
(c) AC welded 4LA **(d) AC welded 4HA**
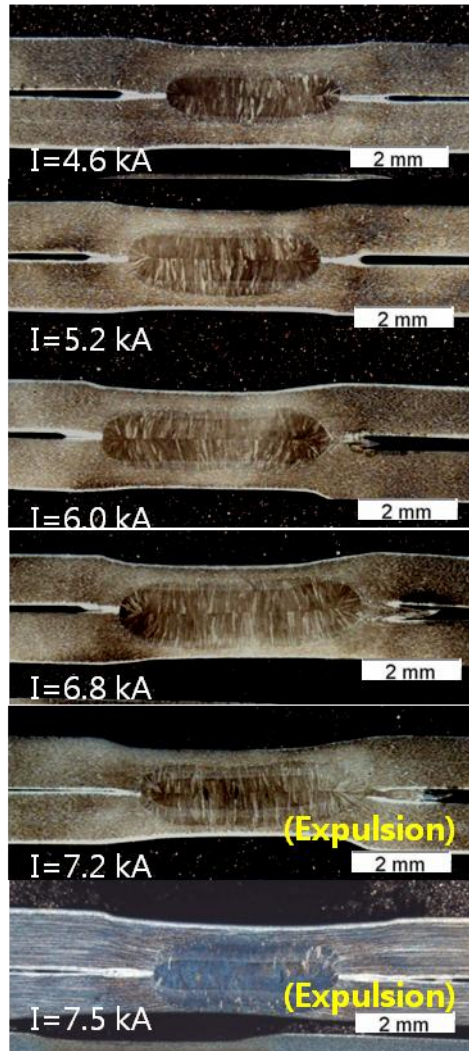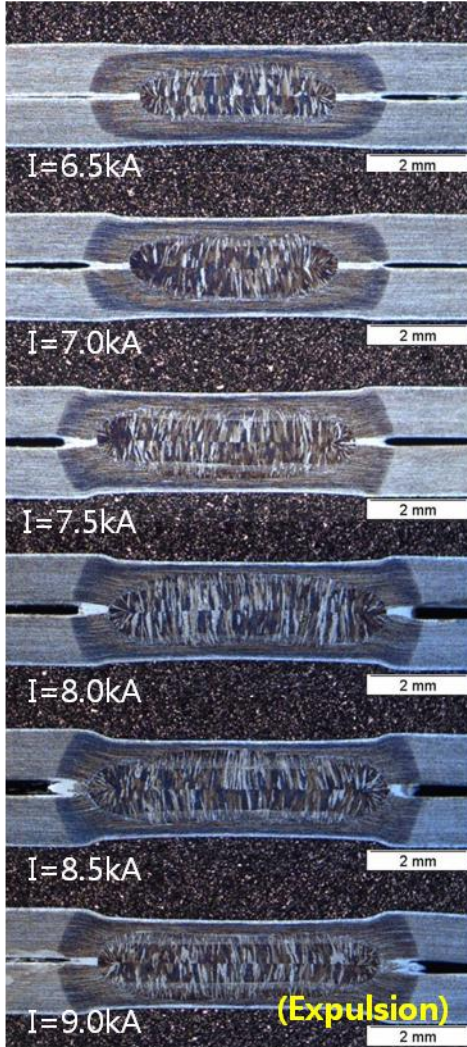
(e) DC welded 3LA　　　　　　**(f) DC welded 3HA**
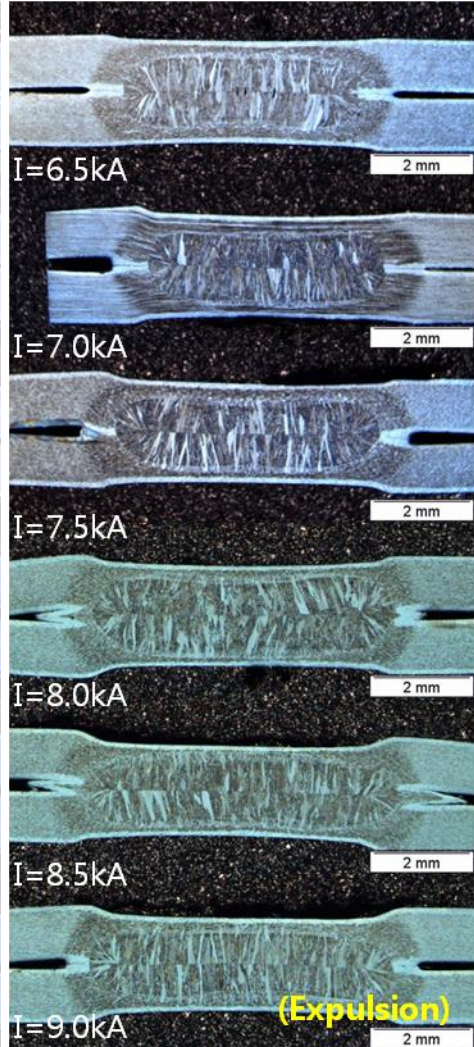
(g) DC welded 4LA   **(h) DC welded 4HA**
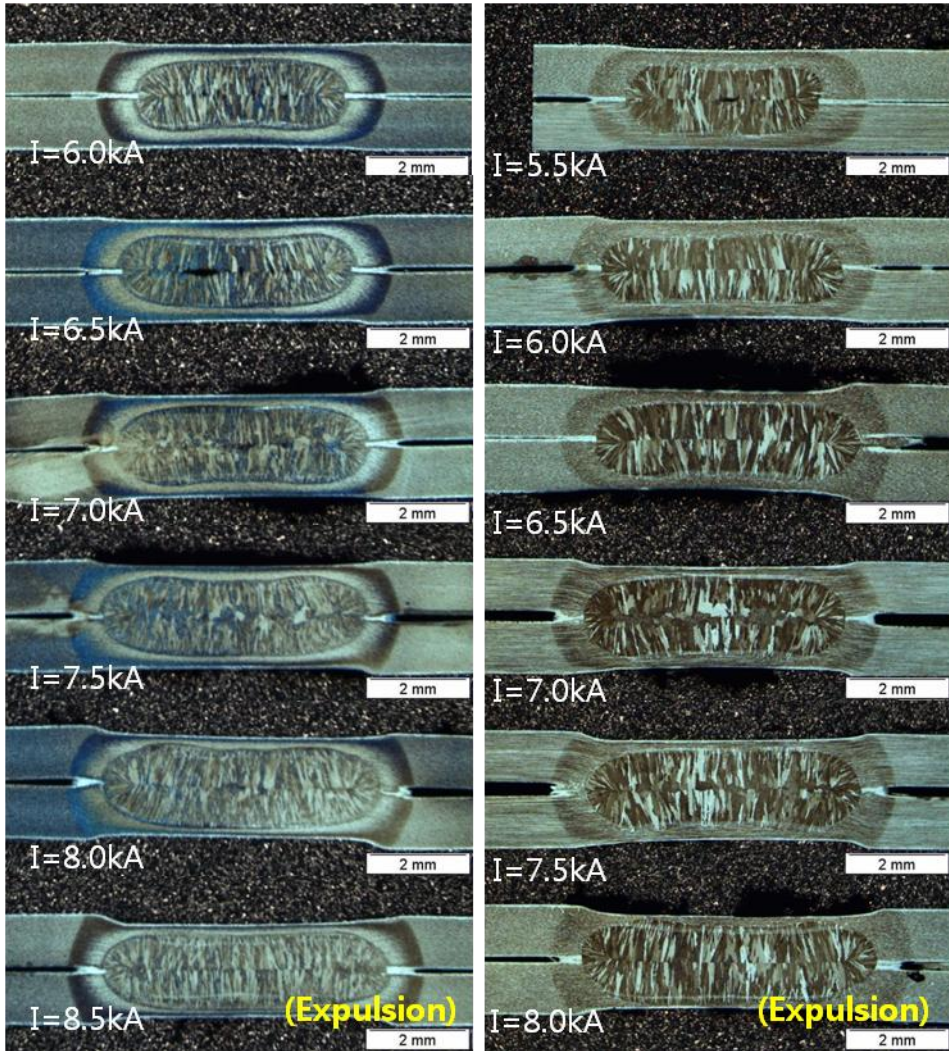
Fig. 5.1 weld nugget growth change of each alloy with different weld currents

3LA weld growth curve

Current type
- AC
- DC

I_{min} (AC)

WS_{min}=4.38 mm

Expulsion

I_{min}(DC)

I_{max}(DC)

Weld size, mm

Weld current, kA

3HA weld growth curve

Current type
- AC
- DC

I_{min}(AC)

I_{max}(AC)

WS_{min}=4.38 mm

Expulsion

Expulsion

I_{max}(DC)

Weld size, mm
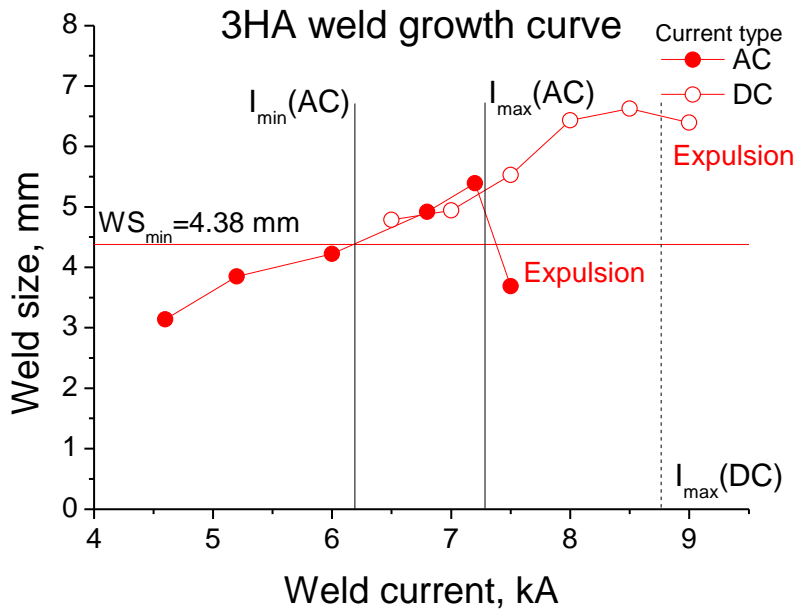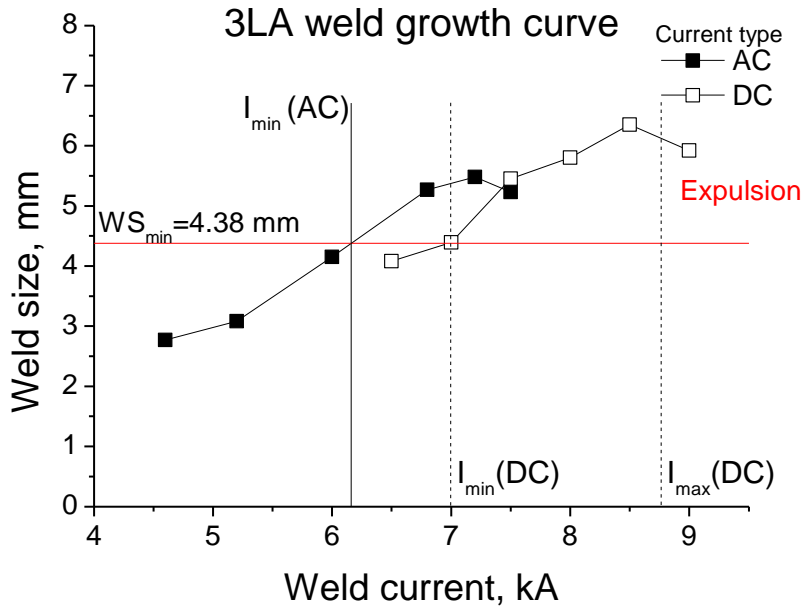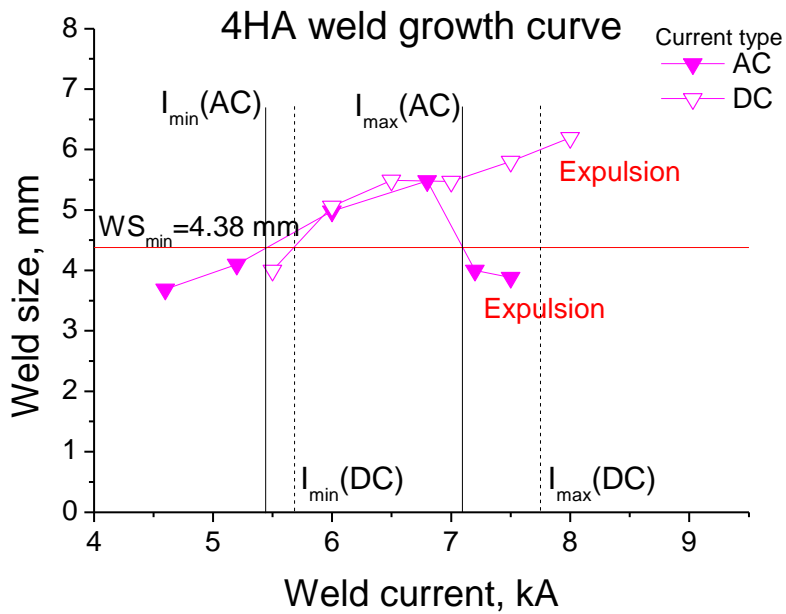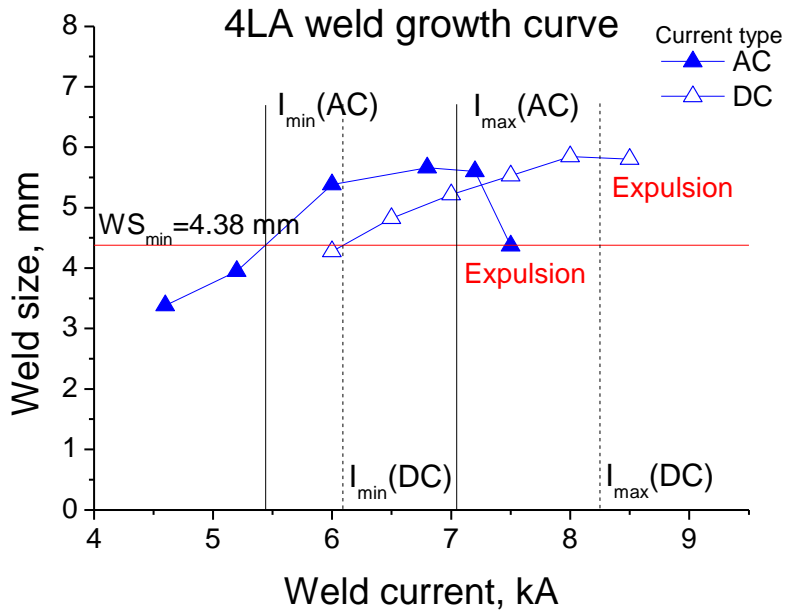
Weld current, kA

Fig. 5.2 weld lobe diagrams for alloys and the weld currents

In Fig. 5.2, both minimum weld current values I_{min}(AC) and I_{min}(DC) were determined from the value where minimum nugget size is produced, and the current value of expulsion was used as an indicator for maximum weld current values, I_{max}(AC) and I_{max}(DC). Generally, I_{max} of steels in this work does not exceed 9 kA, which is disadvantageous for dissimilar welding because mild steels, dual phase steels or interstitial free steels that are used in the automotive industries usually require higher welding currents due to low solute concentrations. It appears that AC welded samples have narrower weld current ranges than those using direct current. And, higher currents are generally required for the DC welding case.

5.2 Weld microstructure

More magnified weld images are provided in Fig. 5.3 and 5.4 for better observation of general weld microstructure and δ-ferrite formation on the solidification in welds. Regardless of weld current types and alloys, δ-ferrite dendrites can be observed in every nugget zone. Even for the case of 4LA, because of very rapid cooling from spot welding process, clear evidence of dendritic δ-ferrite formation was preserved in the microstructure even though the fraction of δ-ferrite was smallest. A point counting method was employed to estimate the δ-ferrite fraction in weld nuggets (Table 5.1). Since δ-ferrite can be retained for every case, fully martensitic nuggets were avoided and thus an improvement of spot weldability is expected.
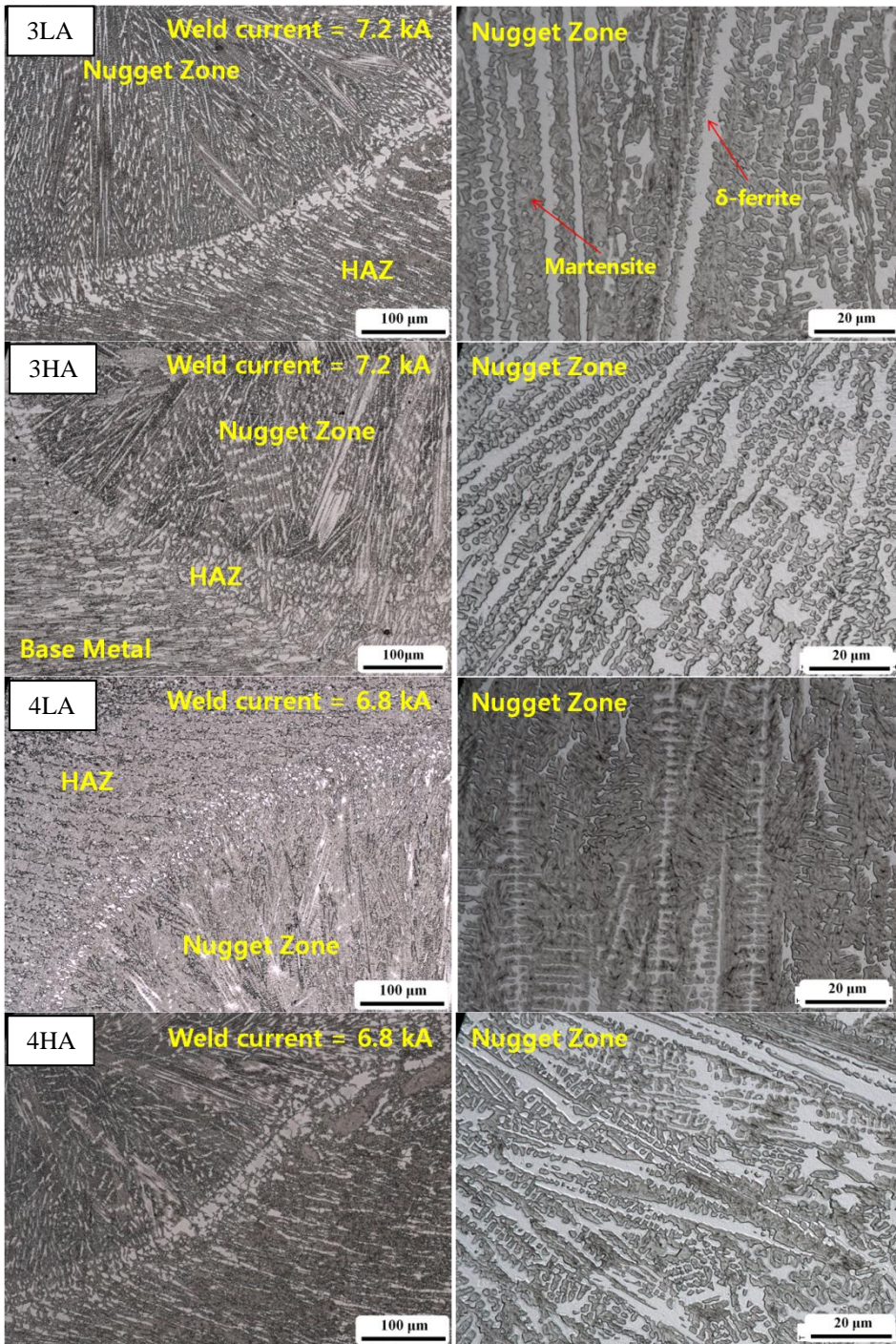
Fig. 5.3 weld microstructure (AC welded)
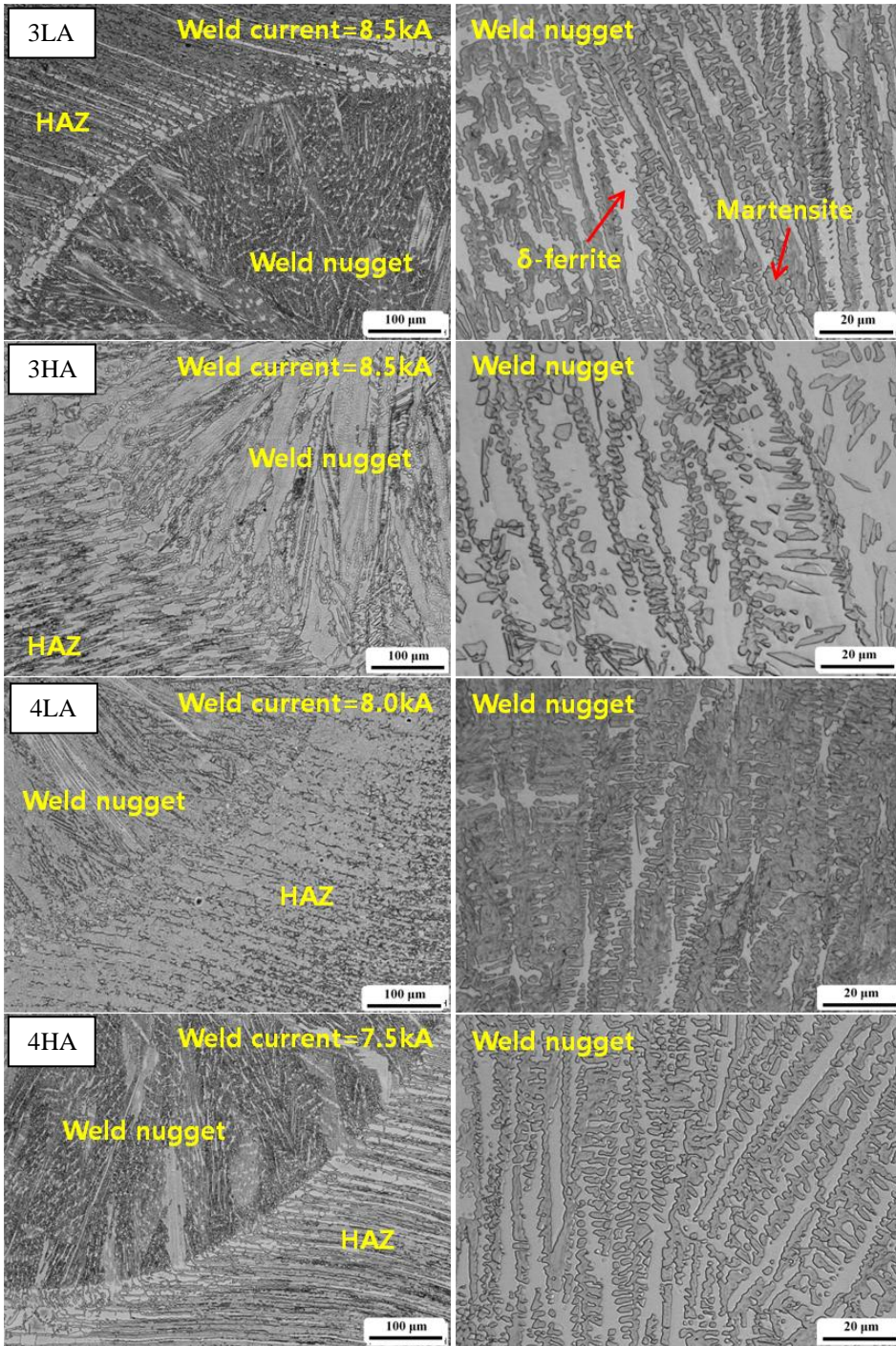
Fig. 5.4 weld microstructure (DC welded)

Table 5.1 δ-ferrite volume fraction comparison in weld nuggets

	3LA	3HA	4LA	4HA
AC	0.27±0.04	0.46±0.05	0.12±0.11	0.37±0.03
DC	0.28±0.03	0.48±0.08	0.19±0.10	0.26±0.07

5.3 Weld hardness

Weld hardness is one of many parameters for evaluation of weldability. For spot welding, because of extremely rapid cooling rate, weld nugget tends toward hard martensitic phase, which is the cause of brittle weld. However, the introduction of soft δ-ferrite is expected to ameliorate this brittleness problem. Hardness was measured across the nugget as illustrated in Fig. 5.5. Fig. 5.6 and 5.7 show the hardness profiles starting from the nugget center to the base metal. The hardness of fusion zone for alloy 4LA is 3 times higher that than of the base metal, and this is due primarily to lack of δ-ferrite. Other alloys show manageably decreased hardness in weld zone, and for alloy 3HA whose retained δ-ferrite fraction is the most the difference is just 1.5 times. Reduced hardness should lead to better mechanical properties by toughening up weld nuggets.
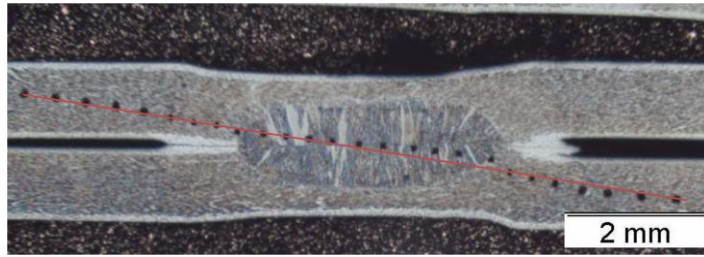
Fig. 5.5 hardness measured across weld nugget
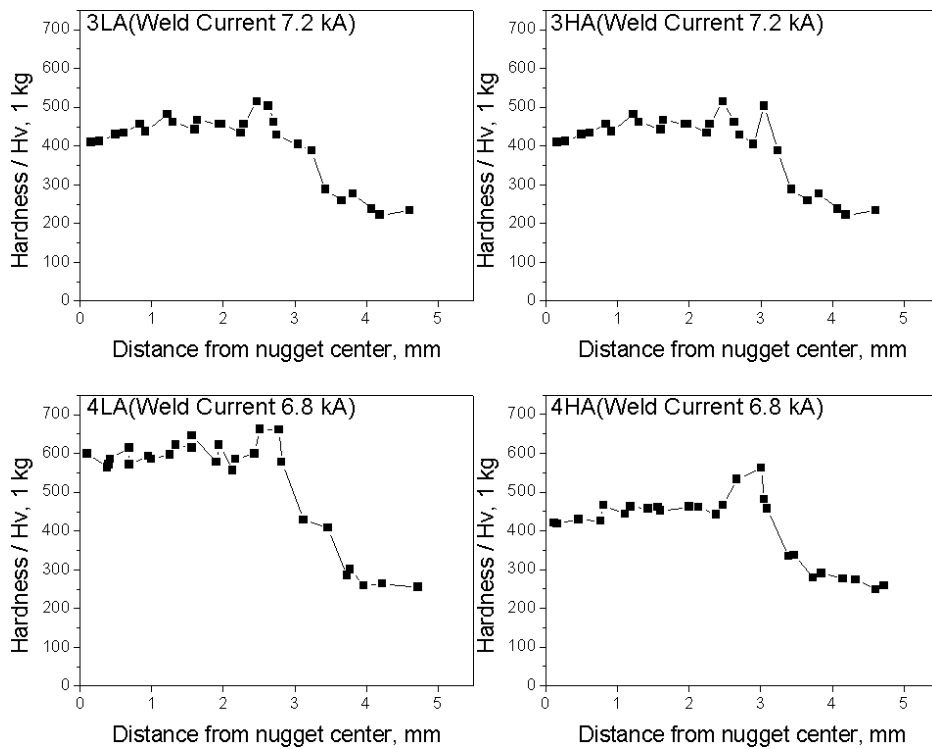
Fig. 5.6 hardness profiles for AC weld (dwell time, 10 s)
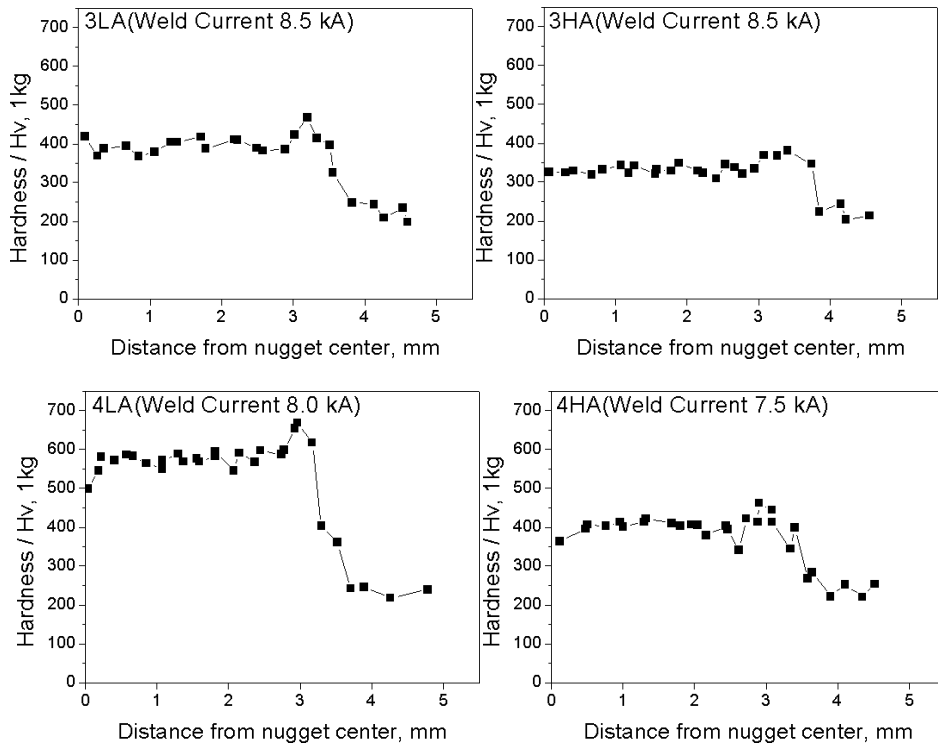
Fig. 5.7 hardness profiles for DC weld (dwell time, 10 s)

5.4 Weld strength

Weld strength was tested by two means according to Japanese standard [53, 54]. Fig 5.10 compares weld strength from AC spot welded specimens, and Fig 5.11 that of DC welded 3LA and 4LA. Overall, the shear strength increases with the nugget size, although cross tensile strength does not seem to respond to the nugget size factor. As a result, the ductility ratio (CTS/TSS) suffers for AC welded specimens. DC welded 3LA and 4LA, nevertheless, shows better ductility ratio due to increased cross tensile strength.
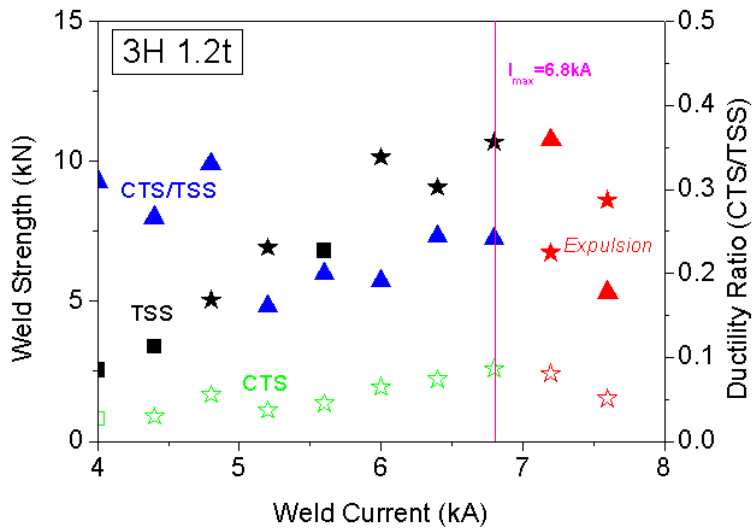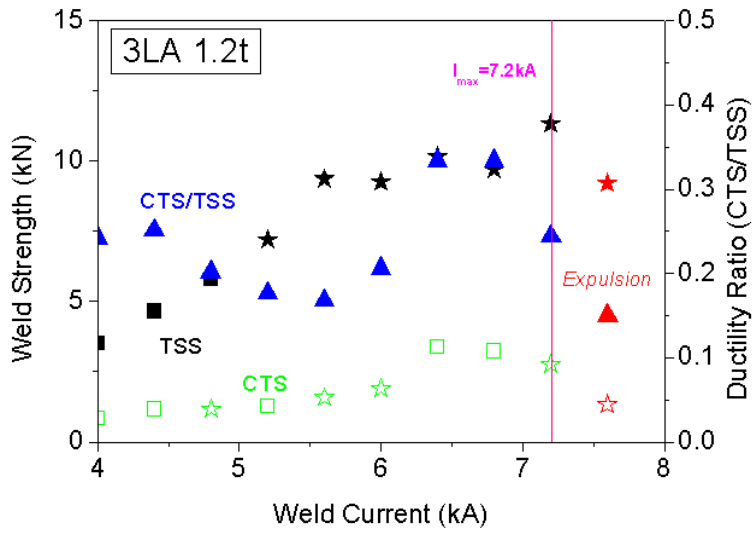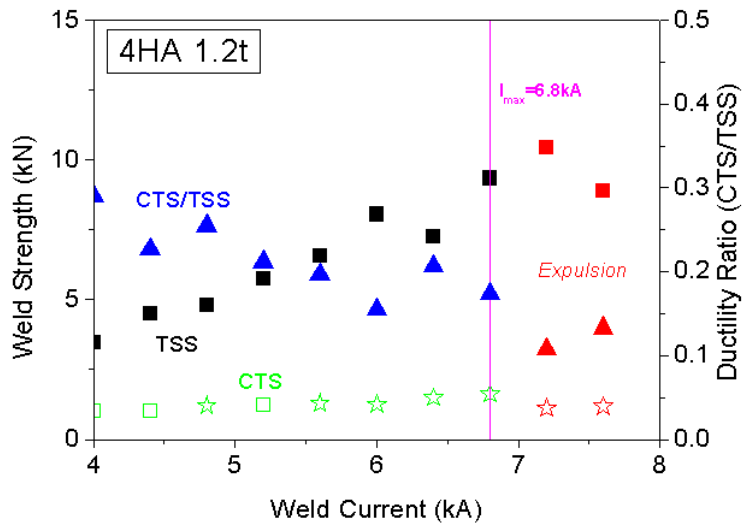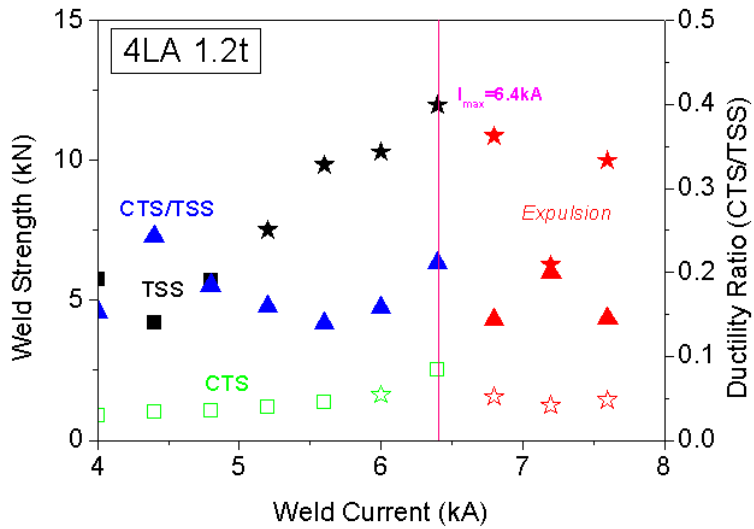
Fig. 5.8 weld strength results for AC spot welded alloys

(■: interfacial fracture mode ★: partial plug fracture mode ●: plug fracture mode)
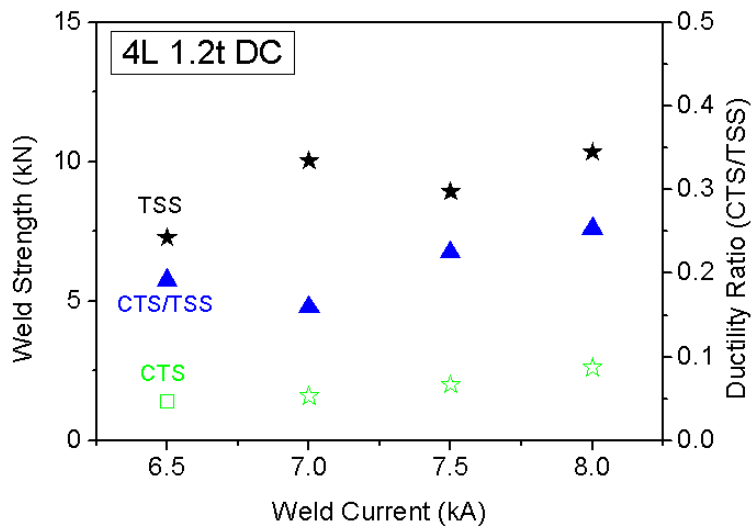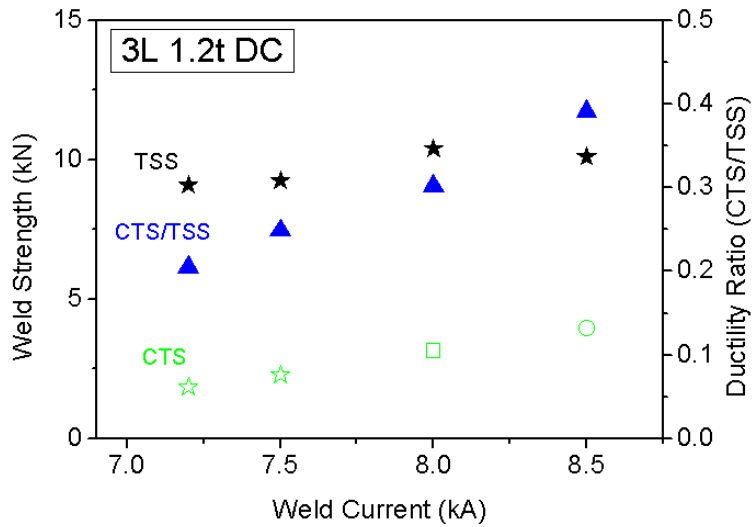
Fig. 5.9 weld strength results for DC spot welded alloys

The effect of electrode force on weld strength was tested and the results are shown in Fig. 5.11. Alloy 3LA was selected and spot welded with DC power

system with one variation, electrode force, changing by 0.5 kN. However, there seemed no remarkable relation between electrode force and weld strength.
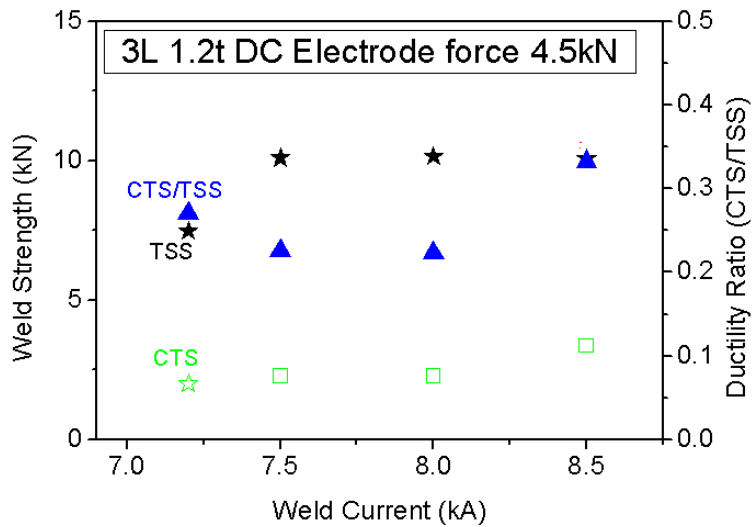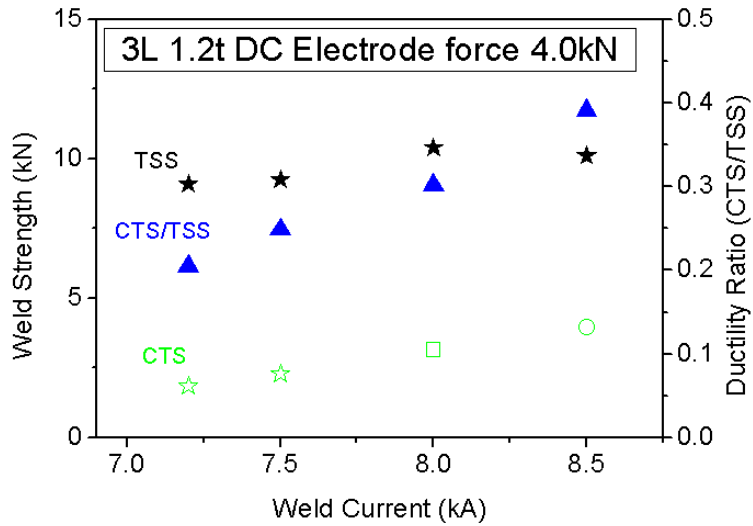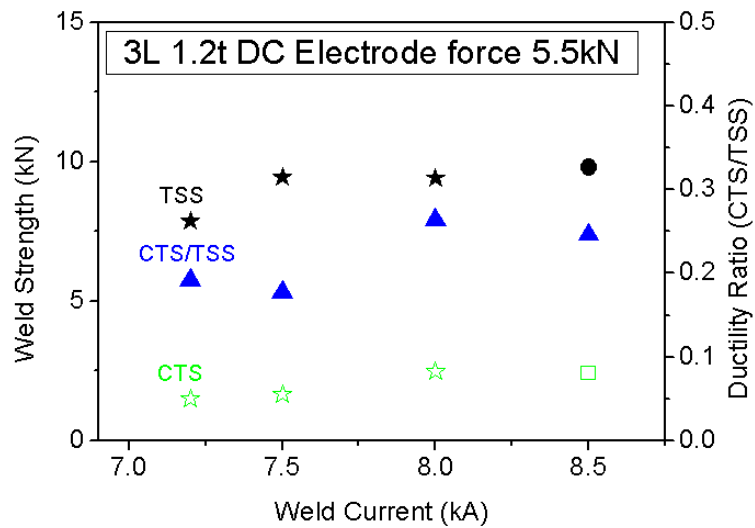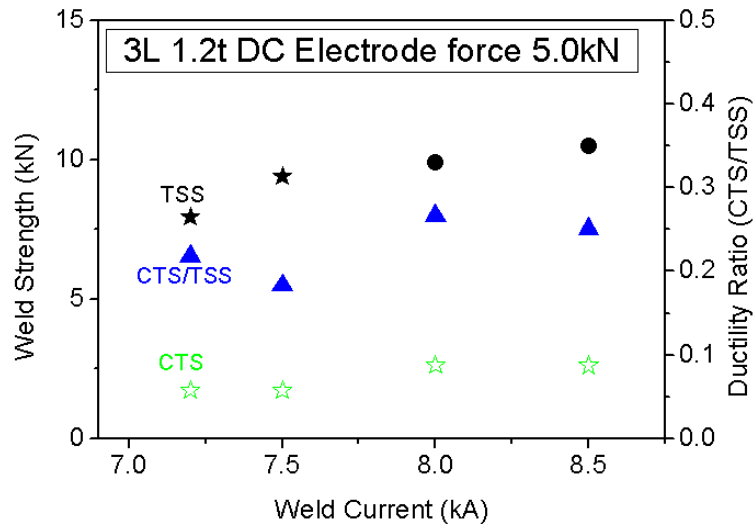
Fig. 5.10 relations between electrode force and weld strength

5.5 Weld fracture surface study

Broken weld nuggets were analyzed for a better understanding of fracture

mechanism. Representative weld fracture images of AC spot welded alloy 4HA are shown in Fig. 5.10. At the center of the weld nugget, A´ in Fig. 5.10 shows evidence of ductile and cleavage fracture at the same time. Along the arrow, dimples, which are indicators of ductile fracture, are found, and it seems δ-ferrite had formed there. In between such dendrites, there is cleavage clearly observed. Thus, two different fracture modes were simultaneously activated during the fracture, which means soft δ-ferrite failed in a ductile fracture mode, while martensite fractured in a brittle manner. Furthermore, around the outermost region of weld nugget, 2 (Fig. 5.10), there can be observed dendrite-shape morphology spreading outward. At heat affected zone, a clear image of massive cleavage region was acquired as shown in '3' in Fig. 5.10. Surface fracture images suggest that hard martensite still causes the problem by breaking in a brittle fashion.

(a) weld fracture surface image of 4HA
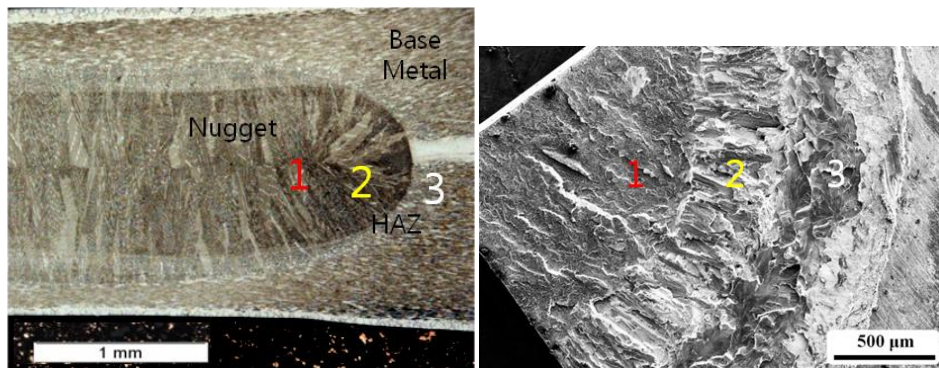
(b) region 1
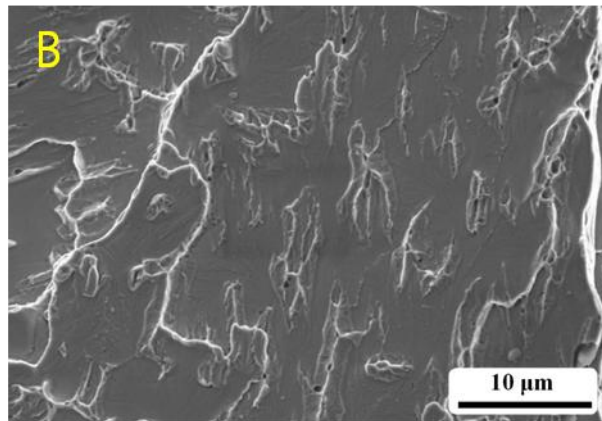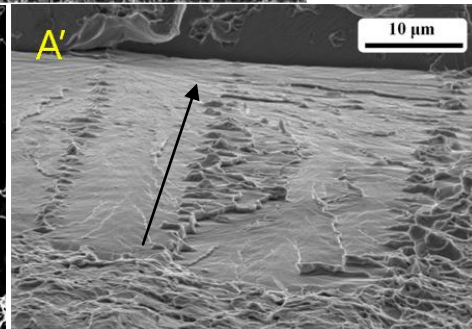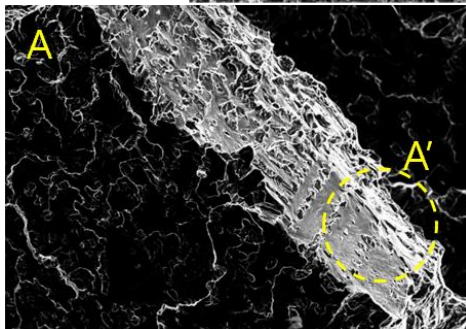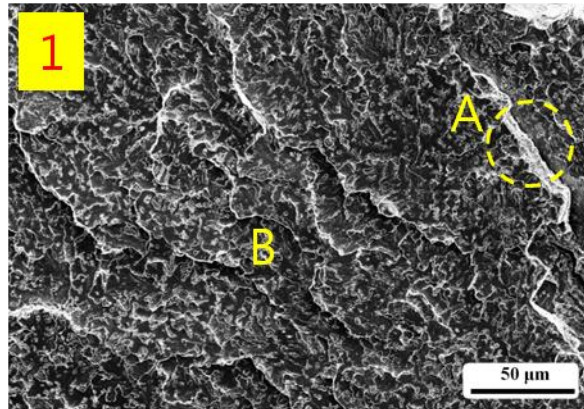
(c) region 2 and 3
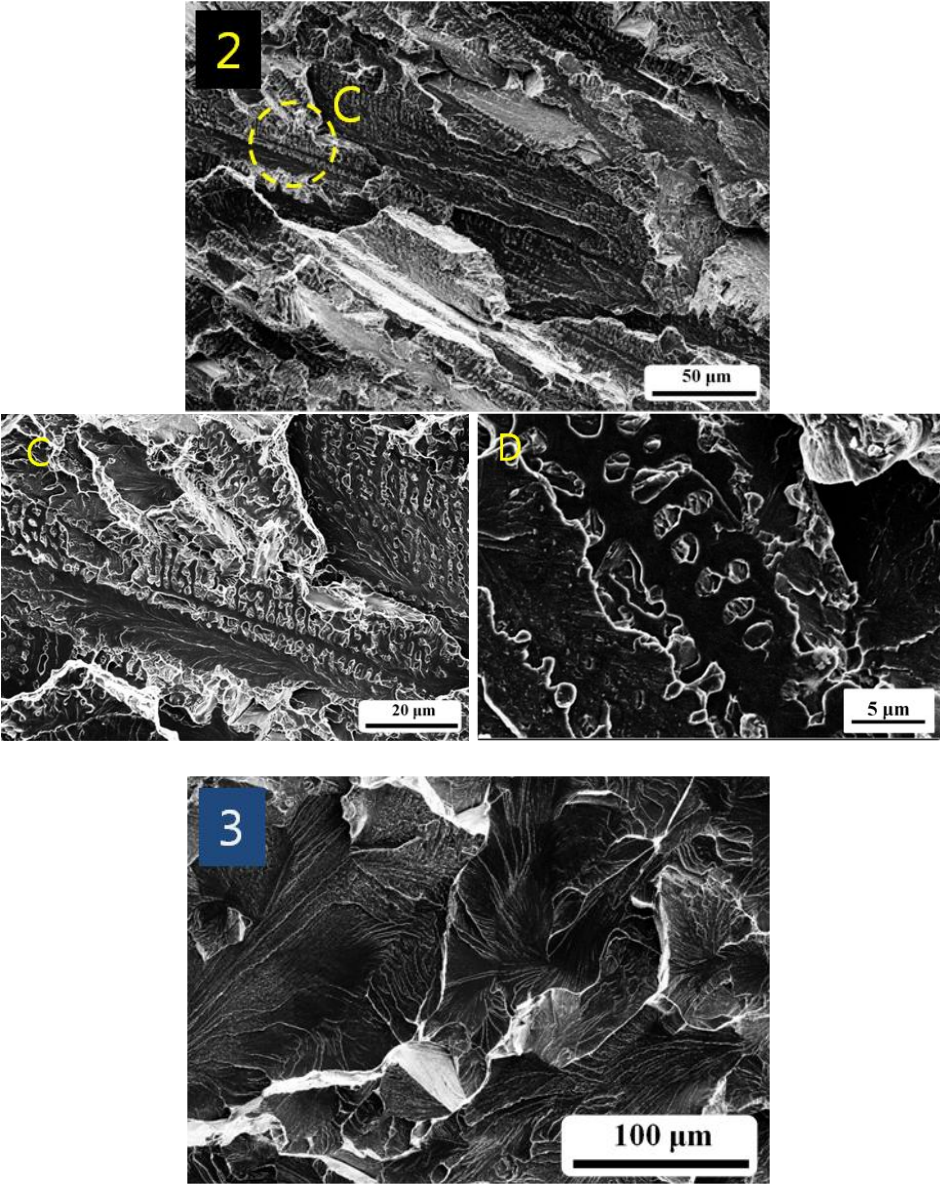
Fig. 5.11 weld surface fracture images of 4HA

5.6 Post weld heat treatment

To deal with the problem of brittleness in the heat affected zone, post weld heat treatment was introduced after welding. Post welding heat treatment is one of popular welding techniques and has been used to remove residual strain or hydrogen trapped in nugget [61]. However, it was not until recently post weld heat treatment technique was tried for resistance spot welding. DC welded 3LA and 4LA samples were selected for post weld heat treatment. Conditions for such heat treatments are shown in Table 5.2. Especially, the second condition was a simulation of the bake hardening process, which is used in automotive production during painting. Remarkable effects were observed especially for 4LA showing ductility ratio reaching 0.4 after post weld heat treatment, which is significant considering alloy composition of 4LA. Low temperature and short duration of heat treatment was rather less effective, but it can be confirmed that the tempering of martensite around weld nugget surely improves weld toughness.

Table 5.2 post weld heat treatment conditions

	Current for 3LA	Current for 4LA	Temperature	time
1	8.5 kA	8.0 kA	-	-
2	8.5 kA	8.0 kA	200℃	30 min
3	8.5 kA	8.0 kA	300℃	1 h
4	8.5 kA	8.0 kA	400℃	1 h
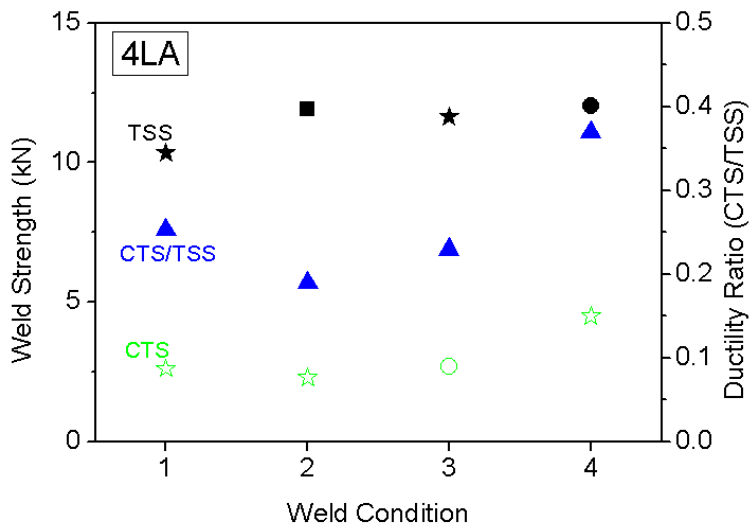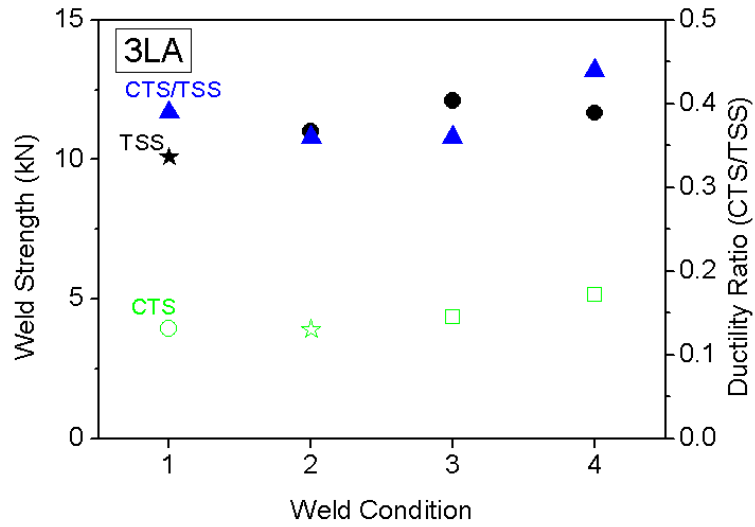
Fig. 5.12 weld strength change after post weld heat treatment

Hardness profiles were obtained for each case, and the results are worth mentioning. In both cases, a reduction of hardness was observed, but alloy 4LA showed a dramatic reduction of 250 Hv in the weld nugget when heat treated with condition 4.
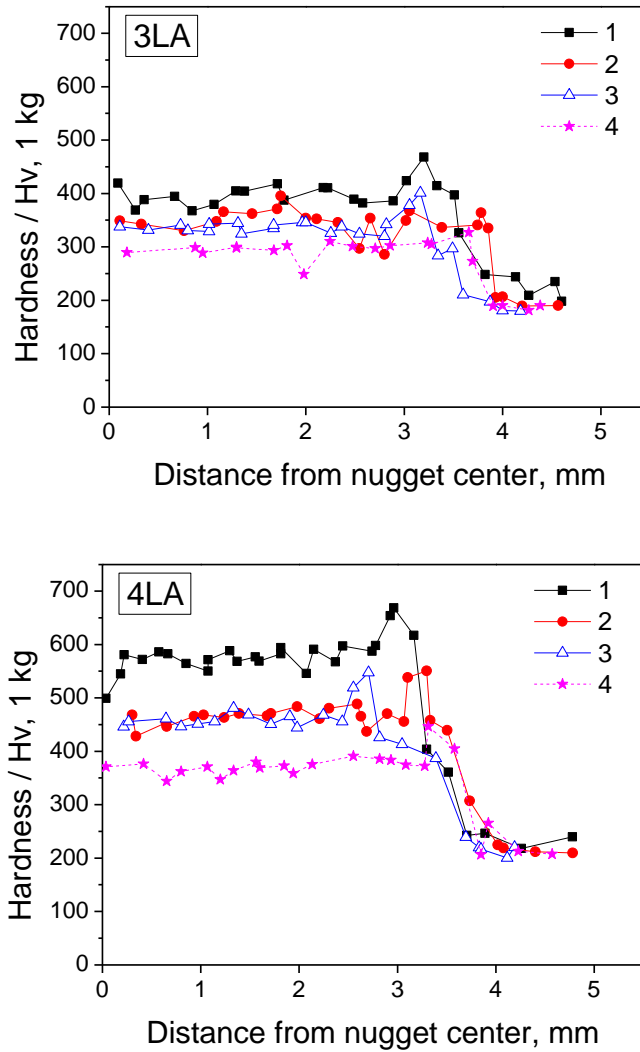
Fig. 5.13 weld hardness profile of 3LA and 4LA after post weld heat treatment

5.7 Weld strength summary

Comparisons for weld strength and ductility ratio are made against commercial steels and previously characterised δ-TRIP steels, Table 5.3. Steels used in this work exceed former δ-TRIP steels in CTS value and ductility ratio even though TSS value seems to be inferior. Compared with current commercial TRIP steels, the performance of steels used for this work is impressive considering the higher carbon concentrations.

Table 5.3 comparison of weld strength and ductility ratio with commercial steels [9, 62]

	Carbon wt%	Minimum weld current, kA	Maximum weld current, kA	Current range, kA	TSS, kN	CTS, kN	Ductility ratio
590DP	0.095	5.0	7.0	2.0	12.2	6.9	0.57
780DP	0.070	4.8	7.6	2.8	15.9	9.4	0.59
780TR	0.155	4.6	7.0	2.4	15.7	5.3	0.34
Alloy8	0.43	-	-	-	16.5	2.0	0.12
Alloy9	0.39	-	-	-	12.5	2.7	0.22
3LAC	0.3	6.2	7.5	1.3	10.9	3.6	0.33
3LDC	0.3	7.0	8.5	1.5	10.1	4.0	0.39
4LAC	0.4	5.5	7.1	1.6	11.6	2.3	0.21
4LDC	0.4	6.2	8.0	1.8	10.3	2.6	0.25

6 Conclusions

The aim of the work was to study the weldability of high strength TRIP steel which, because of the high aluminium concentration, contains δ-ferrite at all temperatures. The possibility for better weldability came originally from this very idea of retaining δ-ferrite in weld nugget which prevents the formation of a fully martensitic weld nugget, thus making the weld nugget better resistant to cold cracking problems.

Prior to the work on welding, the newly designed alloys showed acceptable mechanical properties exhibiting tensile strength of 800 MPa with total elongation of 25%, and further ductility could be acquired at the expense of strength.

For evaluation of spot weldability, two types of resistance spot welding using AC or DC were conducted on alloy samples. In every case, retention of δ-ferrite was possible in the weld nugget, even for alloy 4LA in which δ-ferrite was predicted to completely decompose according to the equilibrium phase diagrams. Based on weld microstructure, suitable welding current ranges were determined for each specimen. Due to the rather high alloy concentration, current levels that are required for welding were in between 5 and 7 kA, which were low and might present difficulties when welded to dissimilar low alloyed steels.

Weld hardness in weld nugget area was effectively reduced to as low as 1.5 times that of the base metal, which accounts for the presence of soft δ-ferrite. Weld strength and toughness expressed by the ductility ratio were also measured.

Tensile shear strength increased with weld nugget size, while cross tensile strength stayed almost the same regardless of weld nugget size changes. Generally, for DC spot welds, the ductility ratio was higher, thanks to better cross tensile strength, although shear tensile strength was not very much different.

From the fracture surface study of broken weld samples, it was determined that martensite, even in the presence of soft δ-ferrite, still showed brittle behavior. As a cure for the matter, post-weld heat treatment on resistance spot welding was suggested, and the ductility ratio as high as 0.45 was achieved through appropriate heat treatment. Although a satisfying level of ductility ratio was achieved, heat treatment, practically tempering, by furnace is deemed counter-productive because of the need for another process after welding. Nonetheless, the significance of welding with heat treatment lies with the conclusion that hard phase martensite was in principle the reason for low cross tensile strength values.

Overall, it is concluded spot weldabilty of TRIP steels can be improved by retaining δ-ferrite in the nugget area because it gives better ductility to the weld. Better weld quality can clearly be achieved with help of heat treatment after welding process even though productivity may be compromised.

References

1. C. Y. Kang, H. J. Kim, C. G. Kim, B. W. Lee, M. Y. Lee, G. H. Lee and T. L. Kim: 'Tensile properties and spot weldability of trip high strength steel sheet', Journal of Korean Society for Heat Treatment, 1998, **11**, 295-304.

2. H. K. D. H. Bhadeshia, R. W. K. Honeycombe: 'Steels: microstructure and properties', 209-233, 2006, Oxford, UK, Elsevier Ltd.

3. B. C. de Cooman, J. G. Speer, I. Y. Pyshmintsev and N. Yoshinaga: 'Materials design - the key to modern steel products', 396-404, 2007, GRIPS media.

4. S. Yoshitsugu, Y. Takako, S. Yoshiharu, F. Sakae and Y. Shu: 'Thermodynamic analysis of selective oxidation behavior of Si and Mn-added steel during recrystallization annealing', ISIJ International, 2009, **49**, 564-573.

5. S. Chatterjee: 'Transformation in TRIP-assisted steels: microstructure and properties', 95-121, Ph.D. Thesis, 2006, University of Cambridge.

6. S. Chatterjee, M. Murugananth and H. K. D. H. Bhadeshia: 'δ TRIP steel', Materials Science and Technology, 2007, **23**, 819-827.

7. H. L. Yi, K. Y. Lee and H. K. D. H. Bhadeshia: 'Stabilisation of ferrite in hot-rolled δ-TRIP Steel', Materials Sciences and Technology, 2011, **27**, 525-529.

8. H. L. Yi, K. Y. Lee and H. K. D. H. Bhadeshia: 'Extraordinary ductility in Al bearing δ-TRIP Steel', Proceedings of the Royal Society A, 2010, **467A**, 234-243.

9. H. L. Yi, K. Y. Lee, J. H. Lim and H. K. D. H. Bhadeshia: 'Spot weldability of δ-TRIP Steel containing 0.4 wt-%C', Science and Techonology of Welding & Joining, 2010, **15**, 619-624.

10. H. L. Yi, S. K. Ghosh, W. J. Liu, K. Y. Lee and H. K. D. H. Bhadeshia: 'Nonequilibrium soldification and ferrite in δ-TRIP Steel', Materials Science and Technology, 2010, **26**, 817-823..

11. 'Handbook for resistance spot welding', 2005, Miller Electric Manufacturing Co., Appleton, WI.

12. D.J. Radakovic and M. Tumuluru: 'Predicting resistance spot weld failure modes in shear tension tests of advanced high-strength automotive steels', Welding Journal, 2008, **87**, 96-s-105-s.

13. H. Oikawa, G. Murayama, T. Sakiyama, Y. Takahashi and T. Ishikawa: 'Resistance spot weldability of high strength steel (HSS) sheets for automobiles', Nippon Steel Technical Report, 2007, **95**, 39-45.

14. T. Saito: 'Resistance Spot welding of high strength Steel', Welding Technology, 1982. **3**(34).

15. S. Brauser, L. A. Pepke, G. Weber and M. Rethmeier: 'Deformation behaviour of spot-welded high strength steels for automotive applications', Materials Science and Engineering, 2010, **527**, 7099-7108.

16. 'Advanced high-strength steel applications guidelines', Auto/Steel Partnership, Southfield, MI, 2008,.

17. S. Thibaud, N. Boudeau and J.C. Gelin: 'TRIP steel: Plastic behaviour modelling and influence on functional behaviour', Journal of Materials Processing Technology, 2006, **177**, 433-438.

18. B. C. de Cooman: 'Structure-Properties Relationship in TRIP Steels Containing Carbide-free Bainite', Current Opinion in Solid State and Materials Science, 2004, **8**, 285-303.

19. O. Matsumura, Y. Sakuma and H. Takechi: 'Enhancement of Elongation by Retained Austenite in Intercritical Annealed 0.4C-1.5Si-0.8Mn Steel', Transactions of the Iron and Steel Institute of Japan, 1987, **27**, 570-579.

20. P. J. Jacques, E. Girault, A. Mertens, B. Verlinde, J. V. Humbeeck and F. Delannay: 'The Developments of Cold-rolled TRIP-assisted Multiphase

Steels. Al-alloyed TRIP-assisted Multiphase Steels', ISIJ International, 2001, **41**, 1068-1074.

21. H. K. D. H. Bhadeshia: 'Bainite in Steels', 129-161, 2001, Cambridge, UK, The University Press.

22. P. J. Jacques: 'Transformation-induced plasticity for high strength formable steels', Current Opinion in Solid State and Materials Science, 2004, **8**, 259-265.

23. J. Mahieu, B. C. de Cooman and S. Claessens: 'Galvanizability of high-strength steels for automotive applications', Metallurgical and Materials Transactions A, 2001, **32**, 2905-2908.

24. P. Drillet, Z. Zermout, D. Bouleau, J. Mataigne and S. Claessens: 'Selective Oxidation of high Si, Mn and Al steel grade during Recrystallization Annealing, and steel/Zn reactivity', Galvatech ´04: 6th International Conference on Zinc and Zinc Alloy Coated Steel Sheet-Conference Proceedings, 2004, 1123-1134.

25. B. Mintz: 'Hot dip galvanising of transformation induced plasticity and other intercritically annealed steels', International Materials Reviews, 2001, **46**, 169-197.

26. T. Maki and T. Furuhara: 'Microstructure and mechanical property of ultra-fine (ferrite+cementite) duplex structure in high carbon steel', Materials Science Forum, 2003, **426-432**, 19-26.

27. M. F. Gallagher, J. G. Speer and D. K. Matlock: 'Effect of annealing temperature on austenite decomposition in a Si-alloyed trip steel', Materials Science and Technology 2003 Meeting, 2003, 563-576.

28. M. de Meyer, D. Vanderschueren and B.C. de Coomaim: 'The influence of the substitution of Si by AI on the properties of cold rolled C-Mn-Si TRIP steels', ISIJ International, 1999, **39**, 813-822.

29. E. Girault, A. Mertens, P. J. Jacques, Y. Houbaert, B. Verlinde and J. V. Humbeeck: 'Comparison of the effects of silicon and aluminium on the

tensile behaviour of multiphase TRIP-assisted steels', Scripta Materialia, 2001, **44**, 885-892.

30.   D. W. Suh, S. J. Park, C. S. Oh and S. J. Kim: 'Influence of partial replacement of Si by Al on the change of phase fraction during heat treatment of TRIP steels', Scripta Materialia, 2007, **57**, 1097-1100.

31.   H. H. Do, K. M. Cho, C. S. Oh, D. W. Suh and S. J. Kim: 'Effects of C Contents on the Microstructures and Mechanical Properties of CMnSiAlCu TRIP-Aided Cold-Rolled Steel Sheets', Journal of the Korean Institute of Metals and Materials, 2006, **44**, 99-107.

32.   M. Zhang, L. Li, R. Y. Fu, D. Krizan and B. C. de Cooman: 'Continuous cooling transformation diagrams and properties of micro-alloyed TRIP steels', Materials Science and Engineering: A, 2006, **438-440**, 296-299.

33.   R. Kuziak, R. Kawalla and S. Waengler: 'Advanced high strength steels for automotive industry: A review', Archives of Civil and Mechanical Engineering, 2008, **8**, 103-117.

34.   D. J. C. MacKay: 'Bayesian Interpolation', Neural Computation, 1992, **4**, 415-447.

35.   H. K. D. H. Bhadeshia: 'Neural networks in materials science', ISIJ International, 1999, **39**, 966-979.

36.   'Epogy 2003', software, 2003, Synaps Incorporation, Atlanta, GA.

37.   M. Hamedi and H. Pashazadeh: 'Numerical Study of Nugget Formation in Resistance Spot Welding', International Journal of Mechanics, 2008, **2**, 11-15.

38.   X. Sun, E.V. Stephens and M. A. Khaleel: 'Effects of fusion zone size and failure mode on peak load and energy absorption of advanced high strength steel spot welds under lap shear loading conditions', Engineering Failure Analysis, 2008. **15**, 356-367.

39.   M. Marya, and X. Q. Gayden: 'Development of requirements for resistance spot welding Dual-Phase (DP600) steels part 1 - The causes of

interfacial fracture', Welding Journal, 2005. **84**, 172-s-182-s.

40. M. Marya and X. Q. Gayden: 'Development of requirements for resistance spot welding dual-phase (DP600) steels part 2: Statistical analyses and process maps', Welding Journal, 2005, **84**, 197-s-204-s.

41. B. M. Brown: 'Comparison of AC and DC rsesistance welding of automotive steels', Welding Journal, 1987, **66**, 18-23.

42. W. Li, D. Cerjanec and G.A. Grzadzinski: 'A comparative study of single-phase AC and multiphase DC resistance spot welding. Journal of Manufacturing Science and Engineering', Transactions of the ASME, 2005, **127**, 583-589.

43. K. Hofman, M. Soter, C. orsette, S. Villai and M. Prokator: 'AC or DC for resistance welding dual-phase 600?', Welding Journal, 2005, **84**, 46-48.

44. H. Zhang and J. Senkara: 'Resistance welding : fundementals and applications', 229-337, 2006, Boca Raton, FL, CRC Press.

45. M. I. Khan, M. L. Kuntz, E. Biro and Y. Zhou: 'Microstructure and mechanical properties of resistance spot welded advanced high strength steels', Materials Transactions, 2008, **49**, 1629-1637.

46. J. Zhang and P. Dong: 'A hybrid polygonal element method for fracture mechanics analysis of resistance spot welds containing porosity', Engineering Fracture Mechanics, 1998, **59**, 815-825.

47. H. Zhang, J. Senkara and X. Wu: 'Suppressing cracking in resistance welding AA5754 by mechanical means. Journal of Manufacturing Science and Engineering', Transactions of the ASME, 2002, **124**, 79-85.

48. J. E. Gould and M. Kimchi: 'Challenges in Welding New Sheet Steel Products', 33rd Mechanical Working and Steel Process Conference Proceedings, 1991. **XXIX**.

49. J. E. Gould, S. P. Khurana and T. Li: 'Predictions of microstructures when welding automotive advanced high-strength steels', Welding

Journal, 2006, **85**, 111-s-116-s.

50. M. Pouranvari: 'Effect of Welding parameters on the peak load and lnergy absorption of low-carbon steel resistance spot welds', ISRN Mechanical Engineering, 2011, 1-7.

51. 'Specification for metal-arc welding of carbon and carbon manganese steels, BS5135, British Standard Institue, 1974.

52. Y. Ito and K. Bessyo: 'Cracking parameter of high strength steels related to heat-affected zone cracking', Journal of Japan Welding Society, 1968, **37**, 683-991.

53. 'Specimens dimensions and procedure for shear testing resistance spot and embossed projection welded joint', JIS Z 3136, Japaneses Standards Association, Tokyo, Japan, 1999.

54. 'Specimens dimensions and procedure for cross testing resistance spot and embossed projection welded joints', JIS Z 3137, Japaneses Standards Association, Tokyo, Japan, 1999.

55. T. Sekita, S. Kaneto, S. Hasuno, A. Sato, T. Ogawa and K. Ogura: 'Materials and technologies for automotive use', JFE Technical Report, 2004, 1-18.

56. International, A., ASTM A370-03a, in Standard test methods and definitions for mechanical testing of steel products.

57. 'Resistance welding – weldability. Part 1: assessment of weldability for resistance spot, seam and projection welding of metallic materials', ISO 18278-1:2004, ISO, Geneva, Switzerland, 2004.

58. 'Resistance welding – weldability. Part 2: alternative procedure for the assessment of sheet steels for spot welding', ISO 18278-2:2004E, ISO, Geneva, Switzerland, 2004.

59. Y. J. Chao: 'Failure mode of spot welds: Interfacial versus pullout', Science and Technology of Welding and Joining, 2003, **8**, 133-137.

60. Y. J. Chao: 'Ultimate strength and failure mechanism of resistance spot

weld subjected to tensile, shear, or combined tensile/shear loads', Journal of Engineering Materials and Technology, Transactions of the ASME, 2003, **125**, 125-132.

61. S. Kou: 'Welding metallurgy', 75-82, 2002, Hoboken, NJ, John Wiley & Sons Inc..

62. 'Automotive steel data book', POSCO Automobile Steel Application Center, POSCO, Pohang, Korea, 2009.

Acknowledgement

I wish to sincerely thank my academic supervisors, Professor Harry Bhadeshia and Professor Dong Woo Suh for their time, guidance and support in the completion of this work. Had it not been for their greatness in the field of material science, I would have not finished this thesis. I am also very much grateful to Professor Jong Bong Lee for his deep knowledge in welding which helped me venture through my research journey. Some of people from POSCO must be recognized as contributors to my thesis. I, especially, would like to thank Principal researcher Kyoo-young Lee and Jr. researcher Sang-Man Yun from Technical Research Labs, POSCO for their support and commitment.

Much appreciation goes to all the members of my group, computational metallurgy group in GIFT, POSTECH, for their help and friendships. Also, I would like to acknowledge some of people from other groups in GIFT who became my best friends and gave me constant mental support. And, all the members from PT group in Cambridge University shall be remembered for their hospitality during my stay in the Great Britain.

Finally, I want to thank my family and friends for always standing by me and believing in me.

Curriculum Vitae

Name: Jung, geunsu

E-mail: geunsrada@postech.ac.kr

Date of birth: 13th July, 1984

Place of birth: Ulsan, South Korea

Education

M. S. 2012, POSTECH (Pohang, Korea), Graduate Institute of Ferrous Technology, Computational Metallurgy Group

B. S. 2010, Changwon National University (Changwon, Korea), Department of Metallurgy and Materials Science Engineering